Piezoceramic Actuated Transducers for Interior Acoustic Noise Control

by

Kimball W. Green, B.S.

Thesis submitted to the Faculty of the
Virginia Polytechnic Institute and State University
in partial fulfillment of the requirements for the degree of

Master of Science

in

Mechanical Engineering

Donald J. Leo, Chair
Ricardo Burdisso
William Saunders

August 2000

Blacksburg, Virginia

Piezoceramic Actuated Transducers for Interior Acoustic Noise Control

Approved by
Advising Committee:

_____

_____

_____

Piezoceramic Actuated Transducers for Interior Acoustic Noise Control

Kimball W. Green, M.S.
Virginia Polytechnic Institute and State University, 2000
Advisor: Donald J. Leo

Abstract

Weight is a critical parameter in the design of any system launched into space. Current launch costs are on the order of 10,000 dollars per pound of payload capacity. Reducing weight and thus increasing payload capacity is always in the forefront of the design process. One method of increasing the payload capacity of launch vehicles is to reduce the acoustic environment in the interior of the fairing. A major problem is that passive methods currently used for noise suppression do not exhibit significant energy dissipation at low frequencies. This motivates the use of active noise control. Using active noise control for frequencies below 200 to 300 Hz in addition to the passive control means has potential to provide broadband noise suppression and thus a smoother, cheaper ride for any payload. The problem with this technique is that active noise control commonly uses electromagnetic speakers as the control element. The weight of the speaker adds more cost to the application due to the approximate cost per pound to send a launch vehicle and payload to space. At 10,000 dollars per pound of payload capacity, the added cost spent on protecting the payload can potentially reduce the amount of payload capacity a customer receives due to monies spent on non-payload mass. Therefore, necessity dictates a light weight noise control solution.

This work investigates the feasibility of a transducer with less mass than that of a conventional loudspeaker which dissipates energy at the acoustic resonances of

an enclosed cavity. The test setup involves using the transducer to lower the sound pressure levels of acoustic resonances which are excited by an external source, thus simulating the launch phase of a launch vehicle. The transducer is used as an actuator to add damping through feedback control.

The transducer is comprised of three thin flexures that are actuated by piezoceramic material attached to both sides. The flexures actuate a speaker cone that is attached to the end of the flexures. The transducer can act as a sensor or an actuator due to the nature of the piezoceramics. The sound absorbing transducer is modeled to couple to the first acoustic resonance of a six foot cylindrical cavity. The cavity acts as a simplified model of a launch vehicle payload fairing. Equations of motion are derived to model actuator motion and the acoustic impedance of the cavity. A state-space model of the system was derived for two cases: a collocated sensor/actuator pair exciting the tube and an external source exciting the tube with the transducer acting as an absorber. The transducer is designed to affect the first mode, however damping is noticed in the next acoustic resonance.

Analysis of the theoretical model indicated up to 70 percent reduction of the open-loop RMS values or a reduction of 10 dB. Experimental results with the optimized transducer produced a 35 percent reduction of the open-loop RMS value or 3.73 dB. The first acoustic resonance coupled well with the first structural mode of the transducer providing optimal noise suppression for the first mode. Damping was also noted in the second acoustic mode. Neglecting the inertia of the tip mass introduced errors in the predictions of the transducer resonances at higher frequencies. This problem limited the ability to control the higher modes of the cavity.

Acknowledgments

First and foremost I would like to thank God for giving me the perserverance to further my education. I would like to thank my advisor, Dr. Donald J. Leo for his wisdom and guidance throughout this process along with the other two members of my committe, Dr. William Saunders and Dr. Ricardo Burdisso. And thanks goes to my parents for their love and support during my years at Virginia Tech.

The experimental work herein was supported by AFOSR Summer Extension Research Program as administered by Research and Development Laboratories, contract number F4999620-93-C-0063; and by the Mechanical Engineering Department of Virginia Tech. Thanks go to Dr. Steve Griffin, our contact at AFRL Kirtland AFB, New Mexico.

Kimball W. Green

Virginia Polytechnic Institute and State University

August 2000

Contents

List of Tables

List of Figures

Chapter 1

Introduction

1.1 Motivation

In launch vehicle payload fairings, the first several minutes of the launch prove critical for sensitive payloads due to the high sound pressure levels associated with liftoff (1; 3). These sound levels range between 120 to more than 150 dB and it is at this point that the payload and the fairing itself are subject to some of the highest levels of vibration and noise the two will see throughout their operating lifetimes (2; 4; 3). In order to avoid over designing payloads such as imaging satellites, space telescopes and military satellites, to withstand these intense levels of acoustic noise, noise absorption methods have been installed. For the mid-frequency to high-frequency noise, acoustic blankets, up to 7.62 cm (3") in thickness, have been deployed (5). Acoustic blankets provide adequate suppression in the mid to high frequency range, but provide less sound absorption at frequencies in which the acoustic wavelength is large compared to the thickness of the material (5). In an effort to achieve broad band absorption by achieving the same level of noise suppression for frequencies below 200 to 300 Hz, active control methods are currently being investigated.

1.2 Conventional Speaker Technology

It has been proven that using conventional electromagnetic loudspeakers as the driver element in an active noise control speaker array, will produce the required levels of noise suppression for a full size payload fairing. A team of Duke University, Virginia Tech, and Dynamic Structures and Materials, Inc. researchers, experimentally found a configuration of eight 20.32 cm (8") subwoofers and the necessary control components that will provide the required stroke of 7.5 mm or 0.295 inches at 28 Hz, and 1.5 mm or 0.059 inches at 120 Hz to provide a 23 percent reduction of the open-loop RMS sound pressure levels, or a 2.3 dB reduction, at 1 volt of disturbance input peak (5).

However, there are several drawbacks associated with using conventional loudspeakers. One problem is that the mechanical resonance of the speaker introduces actuator dynamics that can be problematic for feedback control. Eliminating problems due to mechanical resonance was the basis for work done by Clark and Lane in the development of a 'constant volume velocity source.'They developed a technique for estimating the velocity of an electromagnetic speaker, which reduces the phase lag associated with mechanical resonance (7). The phase lag associated with the resonance can cause stability problems and reduce achievable performance. Another problem associated with this active noise control solution is the weight of the electromagnetic speaker. Electromagnetic speakers gather their name from using a magnet to produce the magnetic field used in conjunction with an electrical signal to move the cone, or piston, up and down. The more stroke of the piston required, usually the bigger the magnet. These magnets along with several other key parts can weigh anywhere from 0.624 kg (1.38 lbs), to 2.89 kg (6.38 lbs), and larger depending on the size of the cone and magnet. In addition to the speaker weight, the amplifier needed to power the speaker has weight penalties associated with it as well. The weight of the configuration designed by the Duke engineers had an estimated weight of 11.33 kg (25 lbs) without a battery and 14.51 kg (32 lbs) with a power supply (5).

As previously mentioned, severe weight penalities are applied to space applications. It costs approximately 10,000 dollars per pound of payload capacity (8). Thus

the above add-on active noise control system's 14.51 kg (32 lbs) will cost approximately 320,000 dollars, which decreases the payload capacity of the launch vehicle. However, if a light weight transducer or speaker could be made that would produce the required amount of stroke needed, the active noise control solution could potentially increase payload capacity.

The control element proposed in this study is purely a transducer. It is not designed for audio reproduction in the same manner as a conventional loudspeaker. The low frequency response for this transducer is on the order of 10 microns, as the piezoceramics are usually more effective at high frequencies, or used in high frequency control applications. Using piezoceramics for low frequency applications at a first thought is useless, because one would believe a piezoceramic will not provide the amount of stroke needed for any type of low frequency control. However, the actuation device for this transducer utilizes the resonance of a beam that is designed to have a resonance at a particular frequency. This gives hope that we can increase the displacement of the transducer in a narrow frequency range for acoustic applications.

This study uses a sealed tube as a simple model of a payload fairing. This may be misleading in the fact that it uses plane waves inside a tube, from which a very small displacement can produce a large sound pressure level. For instance, for a tube five feet in length and six inches in diameter, a displacement of 108 microns at 100 Hz from a piston mounted on the end yields an inner SPL of 120 dB. Once this technology is transferred to a scale model of an actual payload fairing, it may be found that to control the resonances under 300 Hz, larger excursion amounts are necessary than those produced by this tranducer.

Conventional speakers can provide these large excursion amounts, however, the weight penalties associated with the loudspeaker is a drawback. A piezoceramic actuated transducer is lighter in weight than the loudspeaker but provides considerably less stroke. Table 1.1 shows different brands of subwoofers and weights associated with them. Figure 1.1 is a comparison of volume velocity per weight for the two speaker options used by the Duke reseachers versus the piezoceramic transducer designed in this study. Differentiating the speaker displacements (5) to acquire velocity, then

Table 1.1: Speaker data information for various off-the-shelf speakers (courtesy of Air Force).

Brand	Diameter (cm)	Weight (kg)	Weight/size (kg/cm)
Optimus	20.32	1.474	0.073
Optimus	25.4	2.438	0.096
Optimus	30.48	2.892	0.095
Optimus	13.335	0.624	0.047
Fender	16.51	0.822	0.050
Radio Shack	20.32	0.936	0.046
Fender	25.4	1.474	0.058
Radio Shack	30.48	2.155	0.071

multiplying by the volume of air the cone pushes, yields volume velocity. The volume velocity is then divided by mass. This figure shows that although the electromagnetic speakers may produce up to 80 times as much displacement as the piezoceramic transducer, that on a *per weight basis*, the transducer is on a comparable scale. However, due to the low displacements, the absolute volume velocity is still lower than a conventional speakers. The two loudspeakers have maximum excursion levels around 50 Hz where as the transducer is designed to have maximum levels at 100 Hz.

Therefore the electromagnetic loudspeaker and the transducer both have pros and cons. However, motivated by the need for this light weight speaker, this work focuses on the feasibility of a light weight piezoceramic transducer coupled to the acoustic field of an enclosed cavity to see if active noise control methods can be applied.

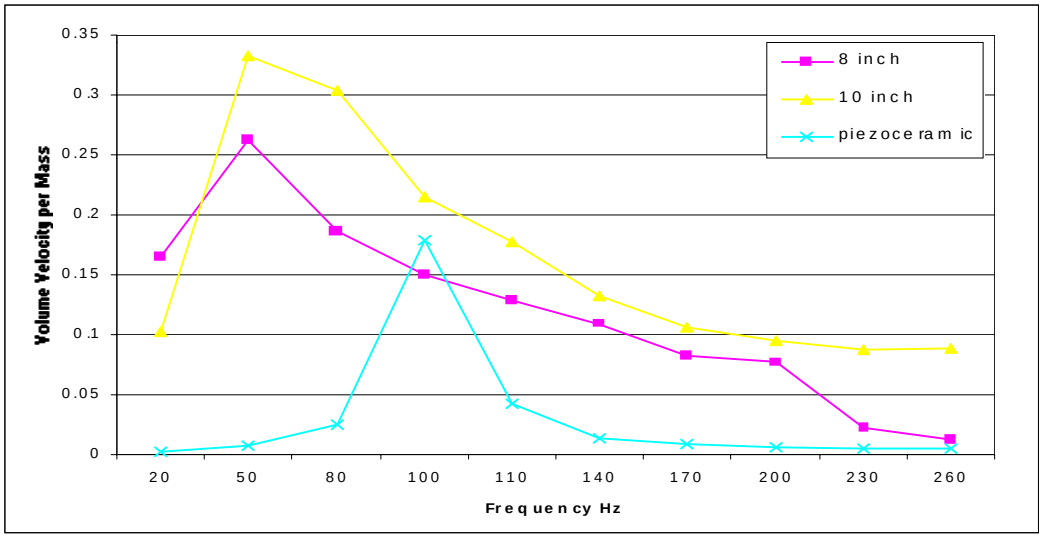

Figure 1.1: Comparison of volume velocity per mass for electromagnetic speakers and transducer.

Figure 1.2: A typical USAF Launch Vehicle Payload Fairing.

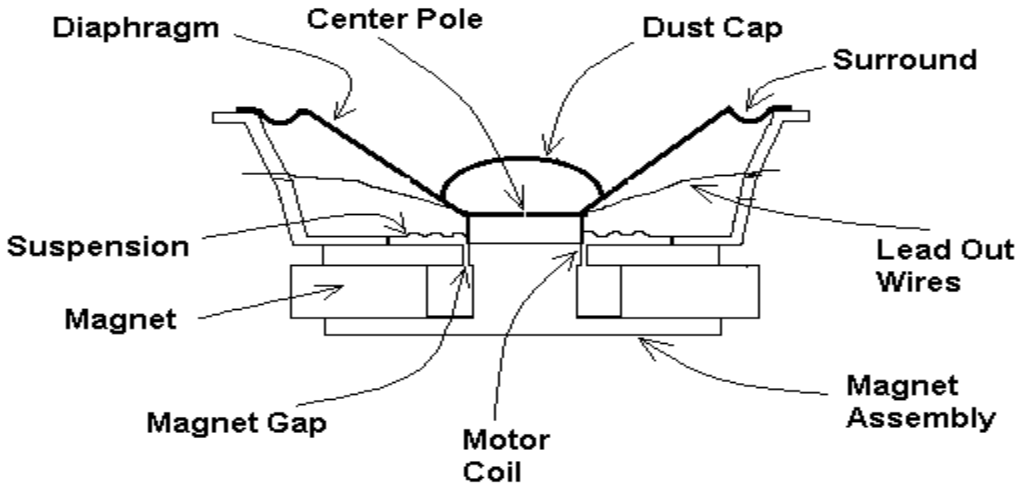

Figure 1.3: Schematic of typical loudspeaker arrangement.

1.3 Literary Review

1.3.1 Electromagnetic Speakers

The conventional electromagnetic speaker has been instrumental in active noise control. The speaker had its first origins in technology generated from electrodynamic principles used in work on the transatlantic cable (9). Edison then created an earpiece which some consider the first ever loud speaker. In the same time frame, Alexander Bell invented the telephone, followed by Ernst Wermer who created the first moving coil loudspeaker. Since then people have attempted to create better, wider range speakers (10). Thanks to Wermer, the basic loudspeaker concept consists of a speaker coil that is wrapped by a predetermined amount of wire which is attached to a cone. The electrical signal is sent through the wire leads. The speaker coil and cone assembly is attached to the housing such that the wire around the coil is centered inside grooves cut into a magnet. The magnet provides a magnetic field that uses the electrical signal to force the cone assembly up and down. Figure 1.3 is a schematic of a typical loudspeaker setup.

To improve and further audio reproduction with the goal of creating a speaker with low distortion and a uniform frequency response, modeling the moving coil

speaker has been a priority. Electrical engineers provided the first models and related the speaker parameters to electrical network theory. In 1954, Beranek (11), presented a comprehensive acoustical circuit derivation for low frequency responses. Others followed with various techniques to model the speaker for a broader range with greater accuracy. All new modeling techniques aided those who began researching Active Noise Control (ANC).

1.3.2 Active Noise Control

Active noise control is an old concept that recently became practical with the advances in signal processing. ANC utilizes engineering-noise control principles, signal processing, and control design techniques to have a means of adapting to different noise sources and using additional sound sources to actively reduce noise levels and in some cases cancel out sound all together. Active noise control was first described in a patent by Lueg in 1933 (22) and since then, numerous others have devoted their research to the further developement of active noise control.

There are many different approaches to active noise control. One such approach is sound field cancellation. This involves using another source signal which is the anti-phase of the original sound. This technique is hard to achieve in a broad band sense, however work has been done to achieve local cancellation (13). A draw back, that is seen in some cases, is that some areas will be magnified outside of the local zone of cancellation. Such local cancellations include the head location of passengers in aircraft and motor vehicles. White created an open-air, active noise reduction headset to be used for such local cancellation and was able to reduce the sound pressure levels by 21 dB (12).

Another technique is what Bies and Hanson calls "suppression of sound generation" (13). This technique is similiar to the above in that it uses out of phase sound to cancel the signal. This method does not cancel the signal but works to change the effective radiation of the original signal, thus making the sound radiation appear to be suppressed.

A third technique, which is the one of interest to this work, is that of sound

absorption. This technique involves absorbing energy from the acoustic field by means of an absorber, such as conventional loudspeaker. This method has its drawbacks in that the control source may only result in sound absorption in the acoustic field close to the absorber if not driven at the proper amplitude. As mentioned in the introduction, this third technique was achieved by Duke University on a full sized 3.66 m (12') tall by 1.37 m (54") in diameter at the base, payload fairing, and was able to achieve global sound absorption.

1.3.3 Feedback versus Feedforward Control

A lot of work has been done in recent years on the concept of feedforward control. Feedforward control is widely used in active noise control when a reference signal, characterizing the primary or disturbance source, is availiable. Feedforward control is characterized by using a fully coherent disturbance signal in conjunction with a feedforward compensator to produce a control signal (15). The compensator is often defined by minimizing the sum of the quadratic square of the signals from error sensors such as accelerometers, for structural dynamics, or microphones, for acoustic dynamics. It was first thought that feedforward control is used to change system zeros and feedback control to change system poles. C. Fuller and R. Burdisso (17; 18) have shown that feedforward can affect the system poles by properly selecting control configurations.

Feedforward control is known to have benefits over feedback control methods (19). Feedforward has a large stability bounds, an error signal that is typically driven to zero, none or very little modeling required, and robustness to model errors (20). However one of the main advantages of using feedback control is that it is more suited to control transient or unknown disturbances. This work uses a random nondeterministic signal to excite the acoustic resonances of a cylindrical cavity. In simulating the real environment, i.e. the launch vehicle, the disturbances will also be of the nondeterministic nature. So efforts in feedback compensator design may be scaled up for a potentially larger application. The main drawback using feedback control is the robustness/stability problems associated with feedback designs (21). For

this application, a stablity problem can potentially increase interior acoustic levels.

1.3.4 Piezoceramics

The history of piezoceramics began in 1880 when the first experimental demonstration of a connection between macroscopic piezoelectric phenomena and crystallographic structure was published by Pierre and Jacques Curie (14). In 1881, Lippmann mathmatecially deduced that the crystals would work in reverse, i.e. producing stress in direct response to an applied electric field. For the next decade, some work took place to understand and further the work with the crystals, but it wasnt until World War I, that the first serious applications were created. Applications such as megacycle quartz resonators, transient pressure measurements tools, and just about all microphones, accelerometers, and so forth that we use today. In 1940, World War II introduced piezoelectric ceramic materials that later advanced into the the lead zirconate titanate, or PZT, that we use today. From 1965 to 1980, the Japanese market advanced the use and commercialized the piezoceramic families to items such as audio buzzers, air ultrasonic transducers, and so forth. Today, the growth of the piezoceramic use is on the rise. One of the more noted uses, is that of active noise control (14).

Piezoceramics are used as actuators in many active noise control applications, and due to the dual nature of the ceramic, it can be used as a sensor as well, thus making a collocated sensor/actuator pair that much more easily done.

1.4 Overview of Thesis

1.4.1 Contribution

This thesis investigates the feasibility of using a piezoceramic actuated transducer to actively suppress low frequency acoustics in enclosed cavities. This research was motivated by the need for a light weight transducer for an active noise control acoustic array to be potentially used in aerospace applications. From this work we hope to gain

an understanding of how to apply modeling techniques to couple structural modes of thin beams to an acoustic field of a cylindrical cavity. Modeled results using Matlab are generated to gain insights on the implementation of feedback control. Difficulties in using pressure as a feedback method versus the use of displacement feedback are discussed. And experimental results are gathered to determine the feasibility of using a transducer actuated by a piezoceramic material as a control element in an active noise control solution.

1.4.2 Approach

Chapter 2 describes the development of the equations of motions for the transducer and optimal design parameters. Chapter 3 details the modeling techniques used and compares theoretical output to experimental output. Chapter 4 describes the design of the transducer. Chapter 5 details control techiques used and experimental results. Finally, concluding remarks and recommendations for future work are given.

Chapter 2

Derivation of Transducer Motion Equations

2.1 Equations of motion

Figure 2.1 is a schematic of the transducer concept. The transducer consists of an acoustic piston and a cylindrical housing. The piston is angled to maximize the stiffness per unit area of the acoustic source. The actuation elements are three piezoceramic bimorphs attached to the bottom of the piston. A single actuator and bimorph is called a flexure. The flexures provide mechanical stiffness to the acoustic source. The complete model of the transducer involves the modeling of three key aspects: flexure model, actuator model, and acoustic impedance model. An external pressure source is also included.

2.2 Flexure Model

The flexures are modeled independently using the assumed modes method. A flexure is assumed to be a thin, flexible beam that satisfies the Euler-Bernoulli assumptions. The following derivation is for one flexure, however, the actual absorber has three flexures. It is assumed that the three flexures will be identical, thus multiplying the mass, stiffness, and actuator moment terms by three to compensate. This assumption

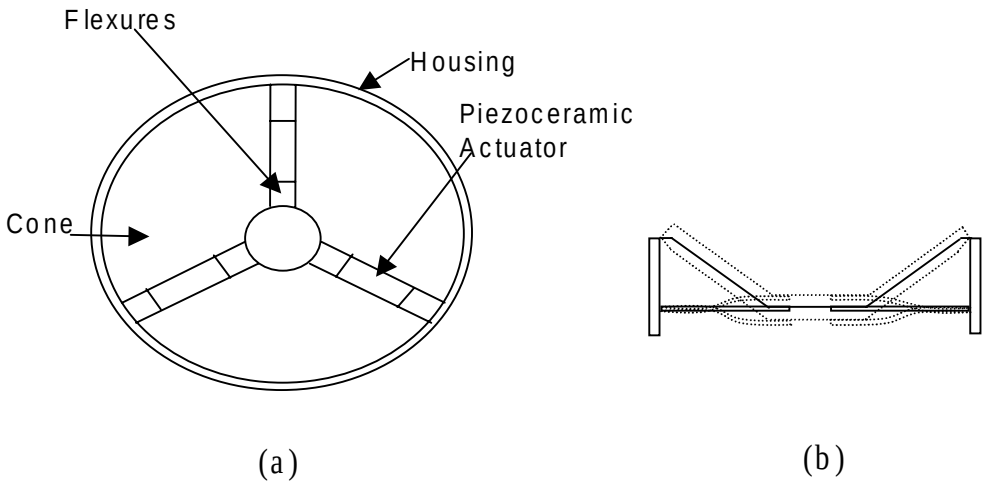

Figure 2.1: Transducer concept illustrating the flexure and actuation mechanisms: (a) top view (b) side view.

appears to be valid and modeling results can be seen in Chapter 3.

The transverse displacement of the beam is denoted *w(x,t)*. The kinetic and potential energy terms for the beam are (23)

$$T = \frac{1}{2}\int_0^L \rho A \left\{\frac{\delta w(x,t)}{\delta t}\right\}^2 dx + \frac{1}{2} m_p \left\{\frac{\delta w(x_c,t)}{\delta t}\right\}^2 \qquad V = \frac{1}{2}\int_0^L EI \left\{\frac{\delta^2 w(x,t)}{\delta^2 x}\right\}^2 dx \tag{2.1}$$

where ρ,A,E, and I are the density, cross sectional area, modulus, and cross sectional inertia of the beam, respectively. The concentrated mass, m_p, models the mass of the rigid piston. Piston inertia and the static load due to the piston are neglected in this formulation, but will be discussed in Section 3.4. The work due to piezoceramic actuation and the external pressure field is expressed as

$$W_{nc} = m_a(t)\left\{\frac{\delta w(x_2,t)}{\delta x} - \frac{\delta w(x_1,t)}{\delta x}\right\} - p(t)A_p w(x,t) \tag{2.2}$$

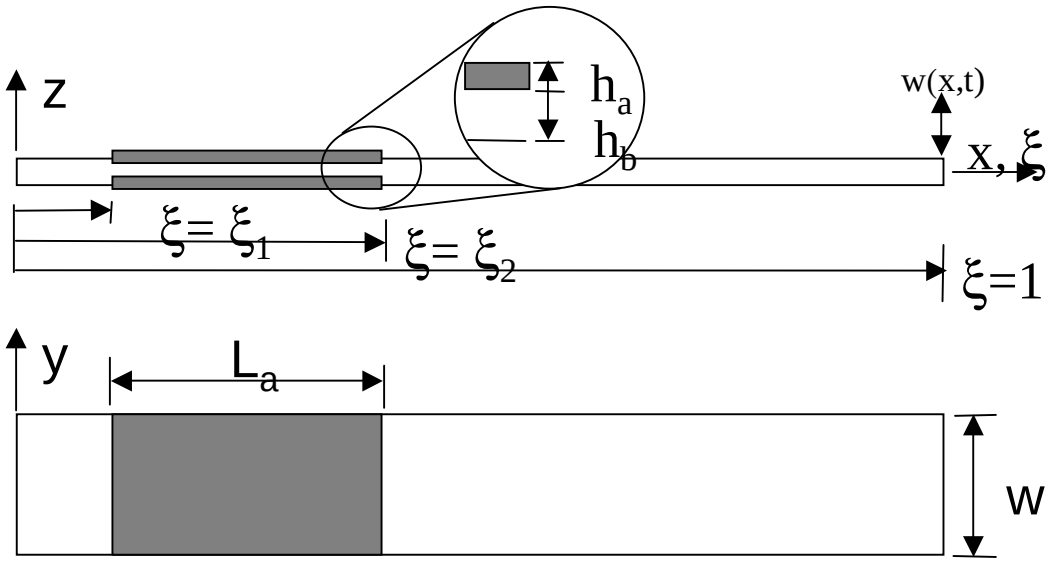

Figure 2.2: Geometry of the beam and surface-bonded piezoceramic.

where $m_a(t)$ is the moment applied by the actuator, *p(t)*, is the uniform back pressure applied to the piston, and A_p is the piston area. Assuming the the displacement w is separable in space and time and expressed as a linear combination of admissible functions $\phi(x)$:

$$w(x,t) = \sum_{i=1}^{N} \phi_i(x) q_i(t) \tag{2.3}$$

where the admissible functions satisfy the geometric boundary conditions of the structure. The flexures are essentially cantilever beams in that one end of the beam is attached to the transducer housing, and the other end is free. By designing the transducer to allow for free lateral movement of the cone, we hold the cantilever beam idea. Therefore, the boundary conditions used for this derivation are for a clamped-free beam and can be found in Inman (23). We can write the kinetic energy expression in matrix form

$$T = \frac{\rho A L}{2} \dot{q}\,(t)^T M_b \dot{q}\,(t) + \frac{1}{2} \dot{q}\,(t)^T M_c \dot{q}\,(t) \qquad V = \frac{EI/L^2}{2} q(t)^T K_b q(t) \tag{2.4}$$

where

$$M_{b_{ij}} = \int_0^1 \phi_i(\xi)\phi_j(\xi)\phi d\xi \quad M_{b_{ij}} = \phi_i(\xi_c)\phi_j(\xi_c) \quad K_{b_{ij}} = \int_0^1 \frac{d^2\phi_i(\xi)}{d\xi^2}\frac{d^2\phi_j(\xi)}{d\xi^2}d\xi \quad (2.5)$$

and $\zeta = \mathrm{x/L}$ is a nondimensional length and $\mu = \frac{m_p}{\rho a L}$. The external work terms can also be written as a matrix expression

$$W_{nc} = \frac{m_a(t)}{L}B_a^T q(t) - p(t)A_p B_p^T q(t) \quad (2.6)$$

where

$$B_a = \left[\frac{d\phi_i(\xi_2)}{d\xi} - \frac{d\phi_i(\xi_1)}{d\xi} \cdots \frac{d\phi_N(\xi_2)}{d\xi} - \frac{d^2\phi_N(\xi_1)}{d\xi}\right]^T \quad (2.7)$$

and,

$$B_p = [\phi_1(1) \ldots \phi_N(1)]^T \quad (2.8)$$

The equations of motion are derived using the Lagrangian formulation:

$$\rho AL\left\{M_b + \mu M_p\right\}\ddot{q} + \frac{EI}{L^3}K_b q = \frac{1}{L}B_a m_a - A_p B_p p \quad (2.9)$$

The (t) notation has been dropped for convenience. This work we will be concerned with the steady state response of the absorber, therefore we transform equation 2.9 into the frequency domain:

$$\left[\frac{EI}{\rho AL^4}K_b - \omega^2(M_b + \mu M_p)\right]Q(\omega) = \frac{1}{\rho AL^2}B_a M_a(\omega) - \frac{A_p B_p}{\rho AL}P(\omega) \quad (2.10)$$

The left-hand side of equation 2.10 represents the mass and stiffness of the flexure and piston and the right-hand side represents the forcing terms due to the acoustic load and piezoceramic actuator. Below is the equation used for the three flexure transducer:

$$\left[\frac{3EI}{\rho AL^4}K_b - \omega^2(3M_b + \mu M_p)\right]Q(\omega) = \frac{3}{\rho AL^2}B_a M_a(\omega) - \frac{A_p B_p}{\rho AL}P(\omega) \quad (2.11)$$

This equation equation is used throughout the modeling of the transducer.

2.3 Actuator Model

The actuators are modeled with the one-dimensional constitutive relationships for a piezoceramic material (24).

$$D_3 = \epsilon_{33} E_3 + d_{31} T_1 \tag{2.12}$$

$$\epsilon_1 = d_{13} E_3 + Y_{11} T_1 \tag{2.13}$$

where ϵ_{33},d_{13}, and Y_{11} are material properties of the ceramic, D_3, is the electric displacement, E_3, is the electric field applied in the z direction, and ϵ_1 and T_1 are the strain and stress, respectively. The applied electric field E_3 is simply the applied voltage divided by the thickness of the piezoceramic, h_a, and the applied stress is equivalent to the actuator force divided by the side area of the ceramic, $\frac{f_a}{w_b h_a}$, Assuming that the strain is equivalent to the actuator extension over the length, x_a/L_a, and intergrating the expression for the electric displacement over x and y yields an expression for the induced charge, q_a, and displacement, x_a, of the piezoceramic:

$$q_a = CV + x_o f_a \tag{2.14}$$

$$x_a = x_o V + \frac{1}{k_a} f_a \tag{2.15}$$

The stress-free capacitance of the ceramic is $C = \epsilon_{33} L_a w / h_a$, the stress-free extension per unit volt is $x_0 = d_{31} L_a / h_a$, and the actuator stiffness is $k_a = w h_a Y_{11} / L_a$. The term $x_o V$ is denoted the free extension because it is equivalent to the actuator extension when the force applied to the ceramic is zero.

The moment induced by the piezoceramic actuators can be written as

$$m_a = 2 f_a \frac{h_b + h_a}{2} = \left[x_o k_a V - k_a x_a \right] (h_b + ha) \tag{2.16}$$

Assuming small deformations and hence small rotation angles, we can write the extension of the actuator as

$$x_a = \frac{h_b + h_a}{2L} B_a^T q \tag{2.17}$$

Equations 2.16 and 2.17 can be combined to yield and expression for the moment applied by the piezoceramic actuator pair. Transforming the expression into the frequency domain yields

$$M_a(\omega) = x_o k_a (h_b + h_a) V(\omega) - k_a \frac{(h_b + h_a)^2}{2L} B_a^T Q(\omega) \tag{2.18}$$

The first term on the right-hand side represents the moment induced by the applied voltage and the second term represents the force applied by the structure on the ceramic.

2.4 Acoustic Impedance Model

The final component of the absorber model is an expression for the acoustic load applied to the piston. We will utilize frequency-dependent impedence models as a means of relating the piston motion to the sound pressure. The use of impedence models makes it straightforward to vary the type of acoustic load presented to the piston. A general impedence model of the load is (11)

$$\frac{P(\omega)}{U(\omega)} = Z_a(\omega) \tag{2.19}$$

where U is the volume velocity of the piston. Assuming that the volume velocity is equal to $Ap\ \dot{w}\ (1, t)$ due to the fact that the displacement of the piston is equivalent to the tip displacement of the beam, we can write

$$A_p P(\omega) = j\omega A_p^2 Z_a(\omega) B_p^T Q(\omega) \tag{2.20}$$

For this work we will assume that the transducer is connected to a cylindrical tube with a rigid end termination. Under this assumption, the acoustic impedence is $Z_a(\omega) = j(\rho_a c/A_p) cot(\omega) l/c)$, where ρ_a is the density of air, c is the speed of sound, and l is the length of the tube. This function can be approximated in the frequency domain as

$$Z_a(\omega) = \frac{1}{j\omega} \frac{\rho_a c^2}{A_p l} \frac{\prod_{i=1}^{N} (1 - \omega^2/\omega_{zi}^2)}{\prod_{i=1}^{N} (1 - \omega^2/\omega_{pi}^2)} = \frac{1}{j\omega} \frac{\rho_a c^2}{A_p l} k_t(\omega) \tag{2.21}$$

For a cylindrical tube with a rigid termination

$$\omega_{zi} = (2i-1)\frac{\pi c}{2l} \quad i = 1, 2.... \tag{2.22}$$

$$\omega_{pi} = i\frac{\pi c}{l} \quad i = 1, 2, ... \tag{2.23}$$

Combining equations 2.20, 2.22, and 2.23 yields an expression for the force applied to the piston as a result of flexure motion:

$$A_p P(\omega) = \frac{\rho_a c^2 A_p}{l} k_t(\omega) B_p^T Q(\omega) \tag{2.24}$$

The term $k_t(\omega)$ is a frequency dependent stiffness that will vary depending on the type of acoustic load that is presented to the absorber.

2.5 External Pressure Source

To model the case with an external source exciting the tube resonances, another pressure term is added to the right-hand side of equation of equation 2.11. Below is the resulting equation with this third forcing term:

$$\left[\frac{3EI}{\rho AL^4}K_b - \omega^2(3M_b + \mu M_p)\right] Q(\omega) = \frac{3}{\rho AL^2} B_a M_a(\omega) + \frac{A_p B_p}{\rho AL} P(\omega) - \frac{A_p}{\rho AL} P_{ext}(\omega) \tag{2.25}$$

The *ext* subscript represents the external pressure input.

2.6 Combined Equations of Motion

The total sytem is now a combination of equation 2.18, 2.24, and 2.25. This system is now a function of the input voltage to the piezoceramics,$V(\omega)$ and the external pressure source, $P_{ext}(\omega)$. The resulting equation is

$$\left[\frac{3EI}{\rho AL^4}K_b - \omega^2(3M_b + \mu M_p) + \frac{3}{\rho AL^2}(k_a\frac{(h_b+h_a)^2}{2L}B_a^T) + \frac{A_pB_p}{\rho AL}(\frac{\rho_a c^2 A_p}{l}k_t(\omega)B_p^T\right] Q(\omega)$$

$$= \frac{3}{\rho AL^2}B_a(x_o k_a(h_b+h_a)V(\omega)) - \frac{A_p}{\rho AL}P_{ext}(\omega) \tag{2.26}$$

Equation 2.26 will be the key equation used in the next chapter to derive the state-space representation.

2.7 Summary

Using equation 2.11, a state-space representation of the transducer is created with two inputs: voltage and pressure. Using equations 2.21 and 2.24 from the acoustic impedence section, a state-space representation which models the resonances of the cavity is used in a feedback loop with the transducer to model the transducer attached to one end of the cavity opposite a rigid termination. Using the external pressure input added in Section 5, we can simulate the launch phase of a launch vehicle, one of the key aspects of this study.

Chapter 3

Modeling

3.1 Introduction

With the equations derived in Chapter 2, a state-space representation of the entire system is derived. This chapter details the open loop system testing and validation as well as closed loop modeling and validation. Explanation behind single-mode testing is discussed.

3.2 State-Space Representation

From the equations derived in Chapter 2, a state-space representation is created. Using state space allows for easily manipulation of the poles and the construction of an observer-based control law. The state-space model for the transducer is shown below. The states used are displacement and velocity of the transducer, x_t and $\dot{x_t}$ respectively, and the equations used are velocity, $\dot{x_t}$, and acceleration, $\ddot{x_t}$. The output is displacement which is fed in a series of poles and zeros which model the tube impedance. It is easy to model any acoustic dynamics of a system with knowledge of the resonances. We can chose the numerator of a transfer function to match the zeros of a system, and chose the denominator to match the poles of the system. Using the TF2SS command in Matlab, which means 'transfer function to state-space', we can convert the poles and zeros listed in equations 2.23 and 2.24 into a state space model.

For this study we used two acoustic poles, meaning two acoustic resonances. The numerical values of this transformation are shown below with the state matrix, x_p. As shown, it has four states, two for each pole. The states are derivative of the pressure of the first acoustic resonance, $\dot{p_1}$, pressure of the first resonance, p_1, the derivative of pressure for the second resonance, $\dot{p_2}$, and pressure of the second resonance, p_2, respectively. The output of the system is pressure over the desired frequency range. This state-space model contains a D term, which has to be accounted for in the over all output matrix for pressure. The D term is a direct transmission of the output from the transducer. This term is key in accurately modeling the pressure inside the tube. The displacement is fed into the pressure model and the output pressure is fed into the input of the transducer. This total system makes up the open loop system shown in Figure 3.2.

$$\begin{aligned} \dot{\bar{x}}_t &= \begin{bmatrix} 0 & 1 \\ A21 & 0 \end{bmatrix} \bar{x}_t + \begin{bmatrix} 0 & 0 \\ B21 & B22 \end{bmatrix} \bar{U}_t \\ y_t &= \begin{bmatrix} 1 & 0 \end{bmatrix} \bar{x}_t + \begin{bmatrix} 0 & 0 \end{bmatrix} \bar{U}_t \end{aligned}$$

$$A21 = -(M^{-1}(\frac{EI}{\rho AL^4})K_b + M^{-1}(\frac{1}{\rho AL^2})BA(k_a(h_b+h_a)^2)BA^T) \tag{3.1}$$

$$B21 = M^{-1}(\frac{1}{\rho AL^2})BA(x_o k_a(h_b+h_a)) \tag{3.2}$$

$$B22 = -M^{-1}A_p(\frac{1}{\rho AL})BP \tag{3.3}$$

$$\begin{aligned} \dot{\bar{x}}_p &= \begin{bmatrix} 0 & -1.7652e6 & 0 & -4.9855e11 \\ 1 & 0 & 0 & 0 \\ 0 & 1 & 0 & 0 \\ 0 & 0 & 1 & 0 \end{bmatrix} \bar{x}_p + \begin{bmatrix} 1 \\ 0 \\ 0 \\ 0 \end{bmatrix} \bar{U}_p \\ y_p &= \begin{bmatrix} 0 & -6.6417e10 & 0 & -3.2241e16 \end{bmatrix} \bar{x}_p + [75251]\,\bar{U}_p \end{aligned}$$

3.3 Open Loop Modeling

The open loop system consists of three stages: speaker model, internal tube pressure feedback, and finally external source excitation. Figure 3.1 shows the conceptual test setup and parameters of which the simulations are based.

3.3.1 Transducer Model

Knowing the characteristics of the speaker is essential in being able to utilize feedback control. Without knowledge of the speaker dynamics, it is very difficult to design the transducer for target frequencies and achieve damping. The transducer for this research utilizes a mechanical resonance of the flexure or beam to achieve maximum stroke. Thus each piezoceramic transducer is targeted at controlling one acoustic resonance. Therefore, it is key that the model accurately represent the dynamics of a given set of parameters or else the speaker design may not control the targeted acoustic resonance.

The targeted resonance in this study is 100 Hz. Using equation 2.23, we can estimate the first resonance of a 1.828 m (6') long tube at 94 Hz. Allowing 7.62 cm (3") for placement of the transducer inside the tube, and reapplying equation 2.23, yields the first acoustic resonance of 100 Hz.

The parameters listed in Table 3.1 are the dimensions used in the model for the transducer. Some dimensions are fixed such as the size of the piston and the length of the beams, which can only be as long as half of the diameter of the tube. Using the state-space model from Section 3.2, Figure 3.3 shows us that the peak resonance of the transducer occurs at approximately 100 Hz with the parameters used in Table 3.1. The model parameters used to produce this model fit well with the specifications that must be met, namely the transducer produced using these dimensions will fit inside the 8" tube that is to be used for the experiment. The static displacement of

Table 3.1: Model parameters used in simulations.

Parameter	Variable	Value
beam modes	mo	1
acoustic modes	po	2
beam length	L_1	8.08 cm (3.18")
beam height	h_b	0.12 cm (0.047")
beam width	b	2.54 cm (1")
beam density	p_{alum}	2.7e3 kg/m^3
length to pzt	x_1	0.8 cm (5/16")
actuator length	La_1	4.13 cm (1.625")
actuator width	w_a	1.89 cm (0.745")
actuator height	h_a	0.027 cm (0.0105")
actuator modulus	Y_{11}	6.2e10 N/m^2
strain coeff.	d_{31}	-320e-12 m/V
cone radius	radius	10.16 cm (4")
cone mass	m_p	0.021 kg
alum. modulus	E	7.31e10 N/m^2
air density	p_{air}	1.16 kg/m^3
speed of sound	c	343 m/s^2
tube length	l	1.81 m (5.95')

the transducer is 0.07 microns per volt and peak displacement is 1.5 microns per volt. In Section 3.3 we discuss the effect of adding more structural modes to the model. However, we can use this model to produce dimensions of a transducer to match one resonance we aim to reduce. The Matlab code used to produce this model is included in Appendix A.

3.3.2 Pressure Feedback Model

Once the model of the transducer is accurate enough to predict the desired resonance frequency, we can model the transducer attached to the end of the cylindrical cavity and begin to predict sound pressure levels. Figure 3.1 shows the theoretical test setup with the transducer attached. As shown in Figure 3.2, to model the internal pressure

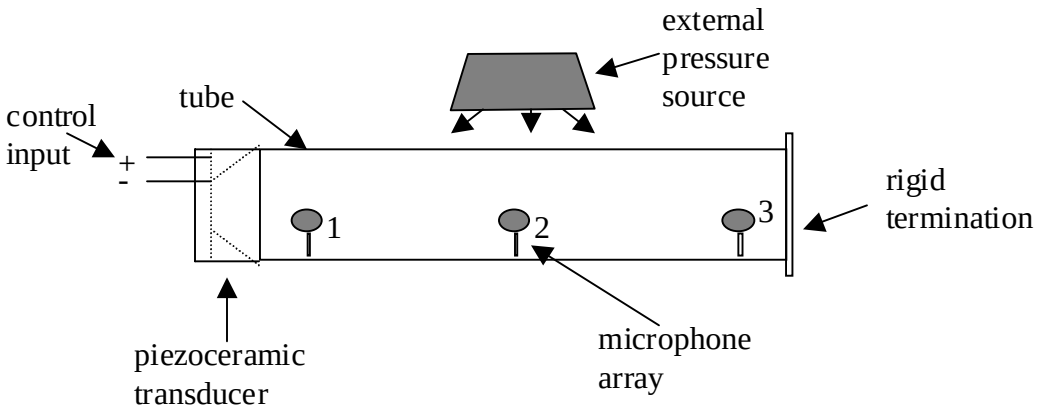

Figure 3.1: Conceptual Test setup.

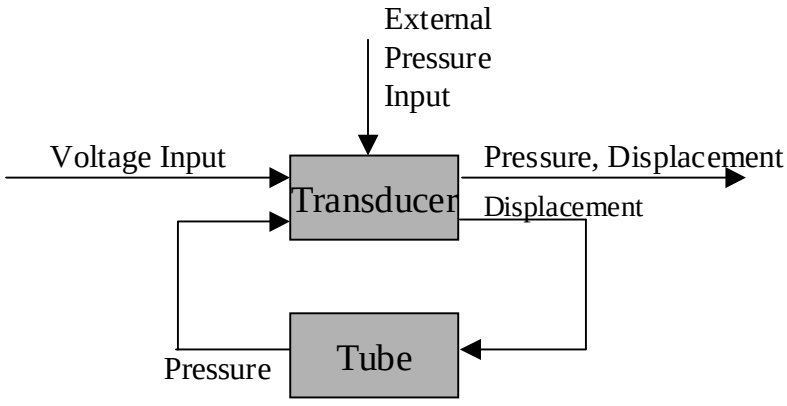

Figure 3.2: Open loop block diagram.

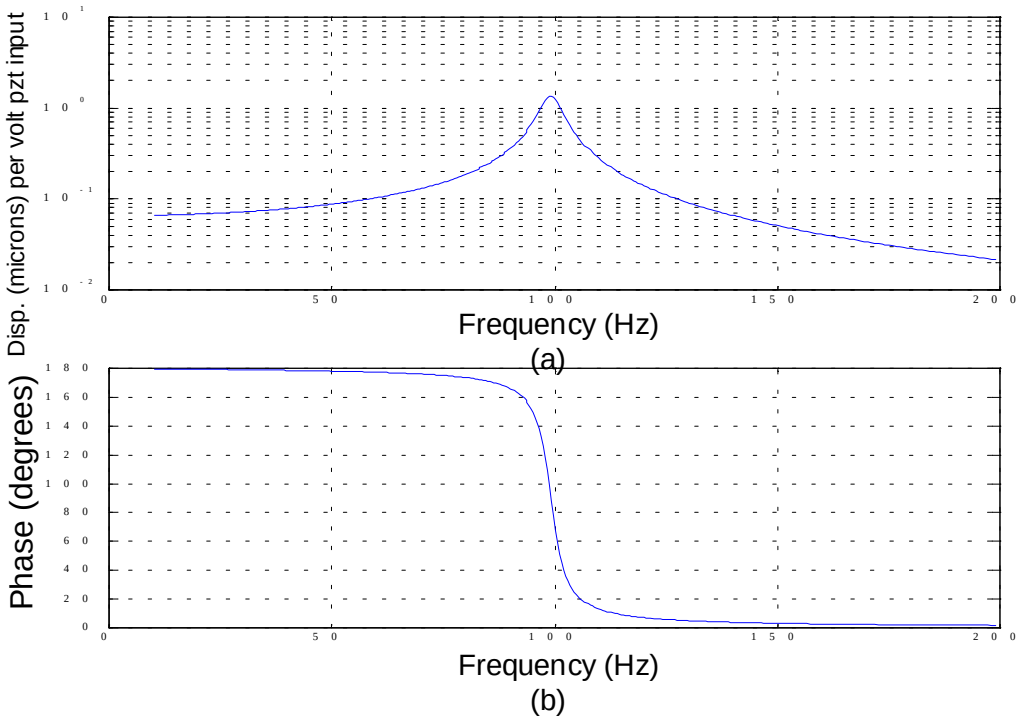

Figure 3.3: Modeled transducer frequency response: a) displacement b) phase.

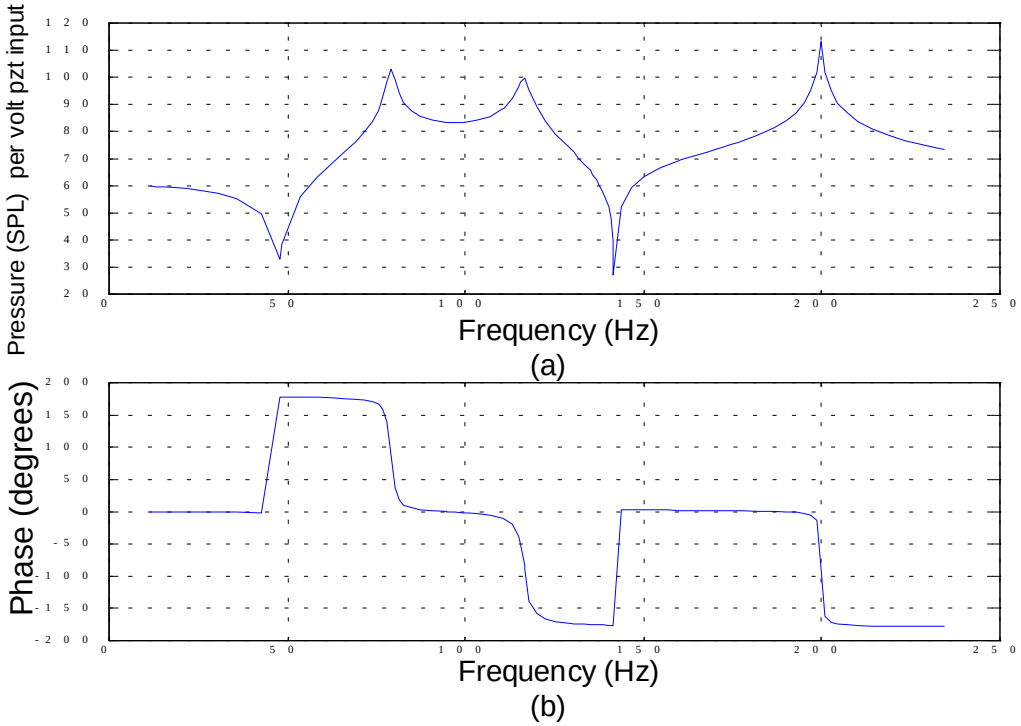

Figure 3.4: Modeled internal tube pressure a) tube pressure in dB b) phase.

dynamics, the state space model of the transducer is placed in a feedback loop with the state space model of the tube dynamics. The tube dynamics, as seen in Section 2.2 and mentioned in Section 3.2, is a series of poles and zeros spaced according to transfer function of a rigidly terminated cylindrical cavity. The resulting system is the new open loop system that describes the internal pressure dynamics of the system. The output of this new system will be total pressure seen inside the tube at the face of the transducer. Any number of acoustic modes may be inputted into the code and analyzed. This model is included in Appendix A.

Figure 3.4 is a plot of predicted acoustic field inside the cavity to excitation of the piezoceramic flexures. This signal will be used throughout the analysis as the control signal: any input to the transducer will produce a similiar response. From this figure it is evident that coupling exists between the designed first structural resonance and the first acoustic resonance. A splitting effect is seen at the first acoustic resonance. In the phase plot, the two new peaks produce a phase lag that transitions from 180 degrees to -180 degrees. This phase lag may be problematic in feedback control.

Figure 3.5 is a plot of predicted transducer displacement with respect to the new tube dynamics that are now seen on the face of the cone. Again it is evident that coupling is present due to the two new peaks seen in the displacement. We can also see that the transducer is coupling to the tube dynamics in the evidence that the second acoustic resonance creates a peak. The phase here exhibits a jump in values for the two new peaks but remains bounded between 0 and 180 degrees. This model is also included in Appendix A.

3.3.3 External Input Model

The external source for this section is modeled as a simple exogenous input that affects all of the pressure modes equally, and a coefficient that takes a pressure input and converts to a force for the structural input. This is done to gain insight on trends that may take place when implementing feedback control. The actual transfer function of the external source is a complicated relationship that requires knowledge

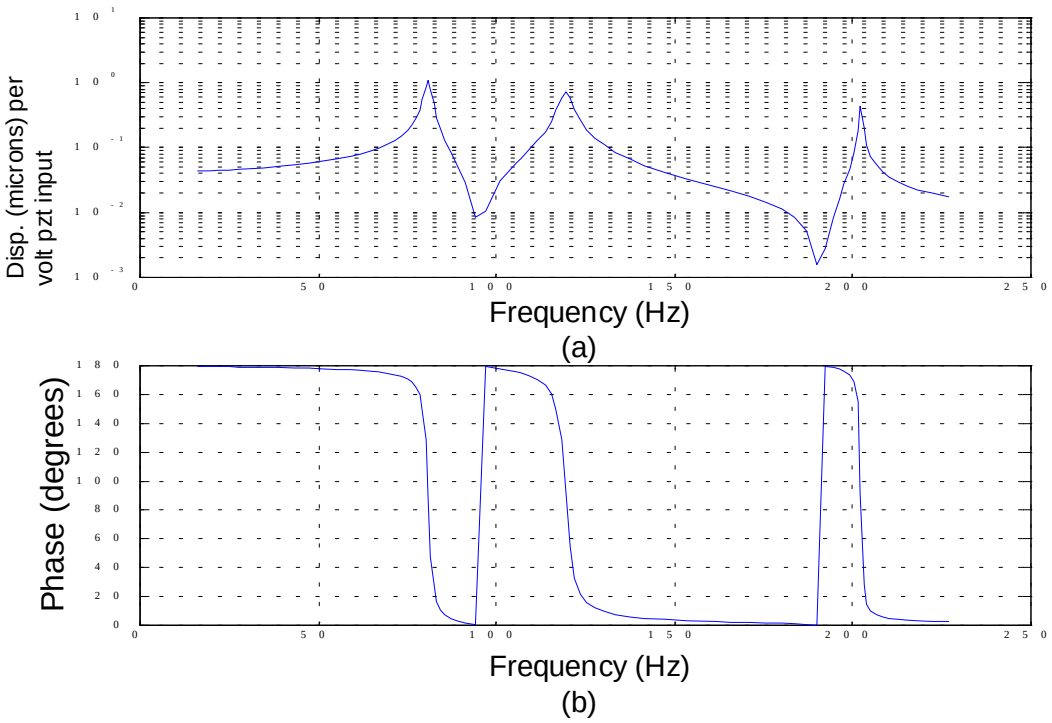

Figure 3.5: Modeled transducer displacement coupled with tube a) displacement in microns per volt b) phase.

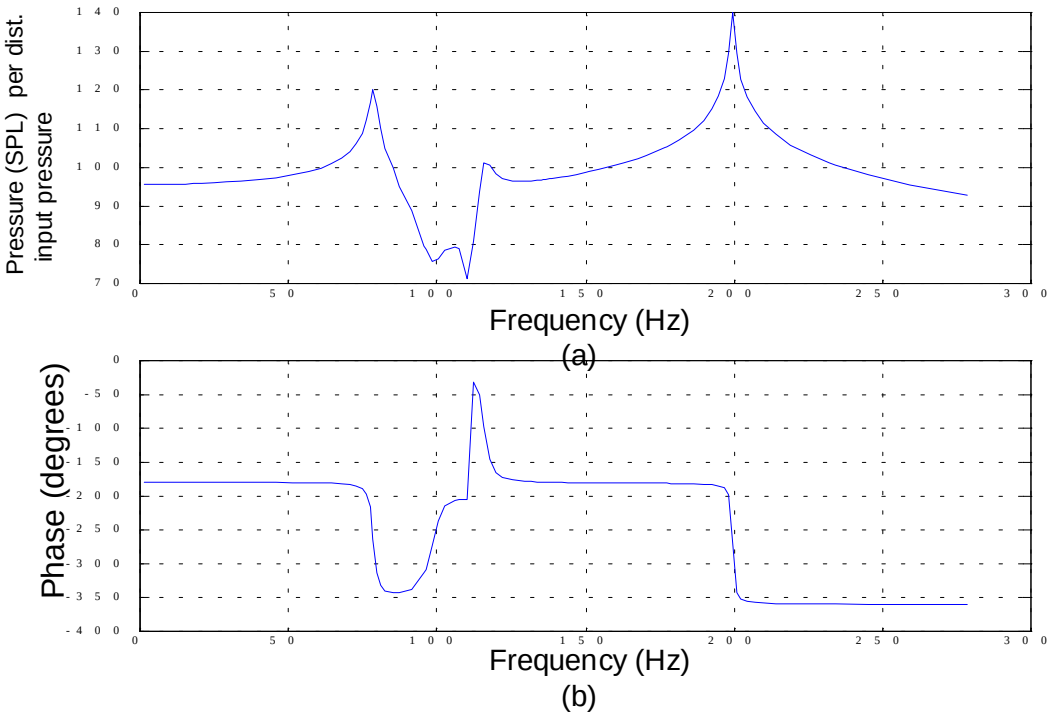

Figure 3.6: Open loop external source input pressure model.

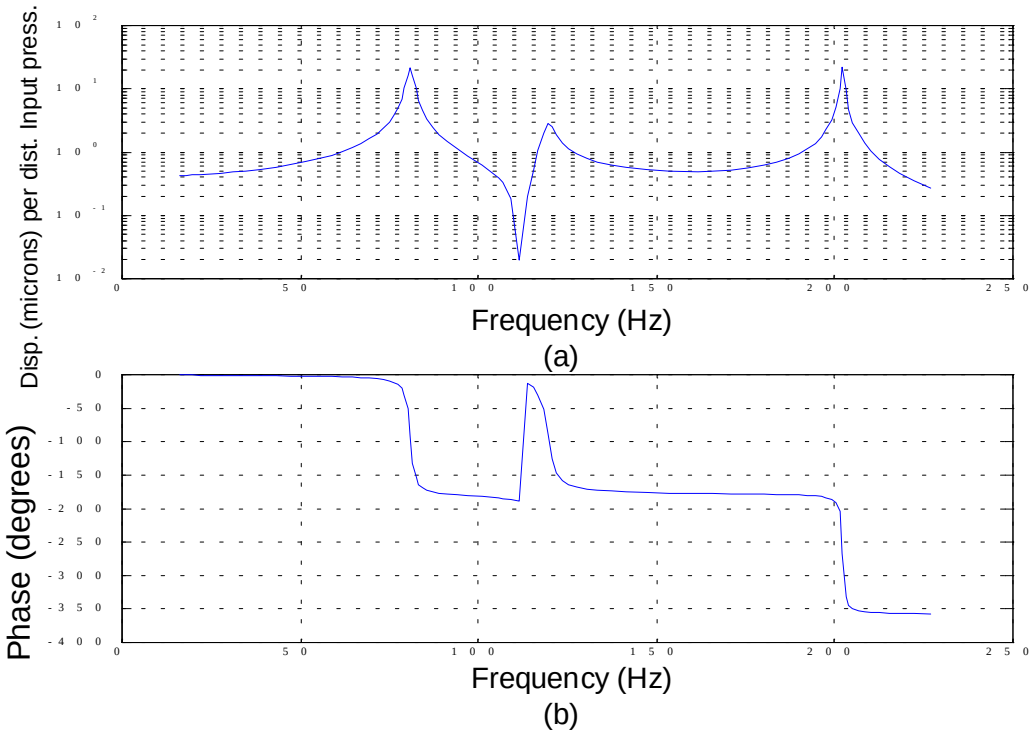

Figure 3.7: Open loop external source input displacement model.

of structural-acoustic transmission of the cavity, transfer loss (TL) coefficients, and T60 times to accurately model the signal going through the tube wall affecting the acoustic resonances of the tube. Time was not spent creating this model due to the concept of a simplified model showing trends that should hold for any external input. However, for future work, creating this intricate transfer function will be suggested.

Figure 3.6 shows the open loop pressure output from the external pressure source. Again the splitting of the resonance at 100 Hz is evident and the second mode is not affected by the transducer. Figure 3.7 shows the open loop displacement of the transducer when the tube is excited by the external pressure source. As with the pressure, the transducer displacement also contains the split peaks around 100 Hz.

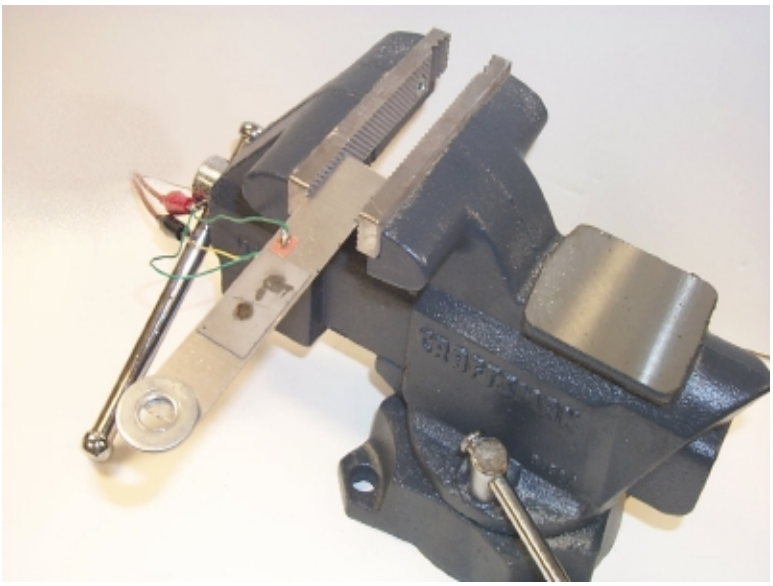

Figure 3.8: Test Setup for Multimode Beam Validation

3.4 Multimode Transducer Modeling

All of the predicted data in the previous sections is for one structural resonance of the flexure. As mentioned in Section 2.2, in the derivation of the equation of motion for a flexure, we chose to neglect the tip mass inertia. In reality, the tip mass does exhibit inertial effects which affect the higher modes of the flexure resonances.

To test the validity of the equation and thus the program, a simple test setup as seen in Figure 3.8 is made. A flexure, with piezoceramics mounted on the top and bottom, is seated into a heavy duty clamp. A hexagon nut weighing 7 grams, approximately 1/3 of the cone mass, is mounted at the tip of the beam standing on a side, approximately 1.27 cm (0.5") high. A random signal with energy up to 5000 Hz is applied to the piezoceramics and the transfer function is taken with a PCB accelerometer, model number U352B22. Figure 3.9 shows the results of the experimental data shown with the predicted transfer function. Notice the model predicts the first mode, then the following modes begin to vary from the experimental data.

In an attempt to determine whether or not having the center of inertia for the tip mass closer to the flexure surface lessens the effect of the inertia, the tip mass

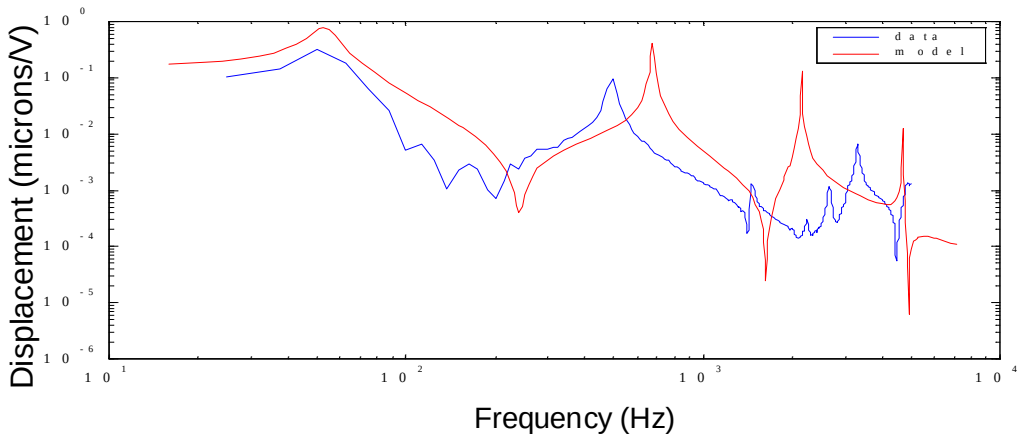

Figure 3.9: Comparision of Experimental Results vs Predicted Results for Beam With Hexagon Nut Mounted on End

on the above beam was changed to a 7 gram washer, mounted flat on the end of the beam. Figure 3.10 shows the results. Again the effects of the tip mass inertia are evident in the experimental results of which the model equations, as is, can not predict.

To validate that the model correctly predicts the dynamics of a bare beam actuated by a piezoceramic, a test was ran with no tip mass. Figure 3.11 shows the experimental results of the same flexure with no tip mass mounted on the end shown with predicted values. First, it is clear that the model accurately predicts this case because there are no inertial effects acting on the tip of the beam. It is also evident that the ratio between the first and second structural modes is still relatively large for the bare beam case. As the beam gets stiffer to couple to a particular frequency, i.e 100 Hz, the ratio becomes larger. With a mass on the end, the distance decreases. However, due to the nature of this research, the goal is to determine the feasibility of a piezoceramic transducer. The approach is to design the absorber to couple to one mode. From Table 3.2 it is clear that even without modeling the inertia effects, the model still predicts the first mode for all three cases. The shear nature of the beam dynamics dictates that the absorber not affect two modes back to back in this particular application due to the distance between the first and second mechanical resonance. However, a one mode approach is accurate from a modeling standpoint

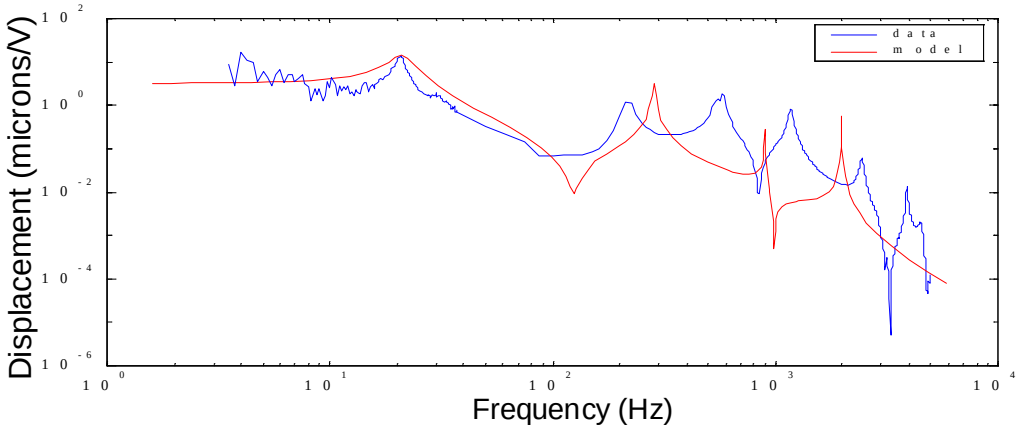

Figure 3.10: Comparision of Experimental Results vs Predicted Results for Beam With Washer Mounted Flat on End

Table 3.2: Summary of multimode results.

	Bare Beam Model/Experiment	Hexagon Model/Experiment	Washer Model/Experiment
1st mode	102 / 100	53 / 55	21 / 21
2nd mode	690 / 700	690 / 490	280 / 210
3rd mode	1095 / 1095	2050 / 1250	900 / 560
4th mode	3800 / 3800	4700 / 3100	2000 / 1100

and is sufficient if an array of these piezoceramic transducers is used to suppress several modes and achieve broad band low frequency noise suppression.

3.5 Close Loop Modeling

This section develops the closed loop form of the system. It places the transducer in a feedback loop with the acoustic impedance then places the open loop system in a feedback loop with a compensator. Figure 3.12 is the block diagram for the closed loop system.

A full state observer is used for pole manipulation to add damping to the

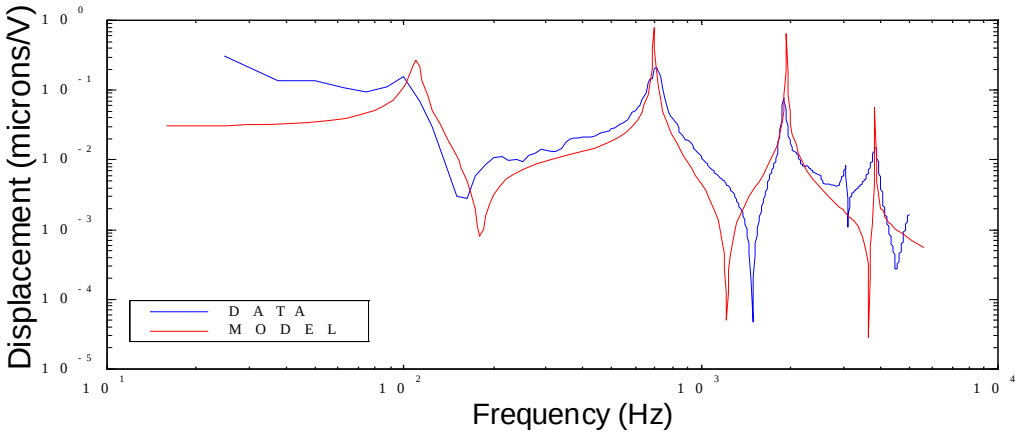

Figure 3.11: Comparision of bare beam transfer function vs. Predicted Transfer Function

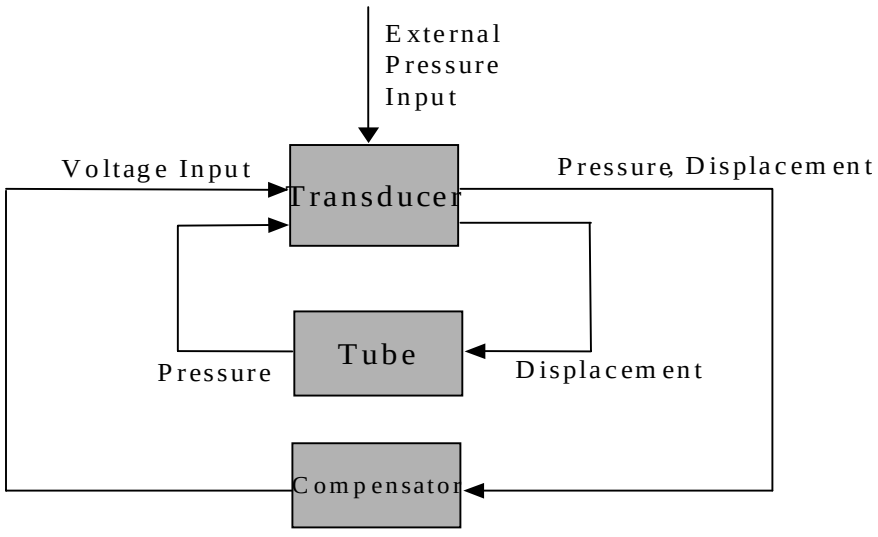

Figure 3.12: Closed loop block diagram.

system. As seen in Figure 3.13, displacement is used as the feedback source. The observer can use a displacement or pressure input, and output a voltage, which is fed into the piezoceramics. The Matlab code used for simulation of the closed loop system is included in Appendix C and the SIMULINK© model is included in Appendix D. Below is the state-space model of the observer (27).

$$\begin{aligned}
\dot{\bar{x}}_{obs} &= \begin{bmatrix} A_{TP} & -B_{TP} * G_{T_{or}P} \\ K_{T_{or}P} * C_{T_{or}P} & A_{TP} - K_{T_{or}P} * C_{T_{or}P} - B_{TP} * G_{T_{or}P} \end{bmatrix} \bar{x}_{obs} + \begin{bmatrix} B_{TP} \\ 0 \end{bmatrix} U \\
y_{obs} &= \begin{bmatrix} 0 & G_{T_{or}P} \end{bmatrix} \bar{x}_{obs} + [0]\, U
\end{aligned}$$

Notice that each variable in the model has a subscript. The TP indicator describes the open loop matrix that combines the dynamics of the transducer, T, and the impedance terms, P. The other terms have a T or P subscript that indicates that if displacement is chosen as the feedback term, the T for transducer is used. P is used for pressure feedback. We can use displacement or pressure feedback simply by changing the output matrix to either represent transducer displacement or pressure seen at the transducer face.

As seen with the open loop model, the acoustic resonance at 100 Hz is split by the transducer, and the two individual peaks exhibit the added damping. Figure 3.13 shows the results of adding damping to the crudely modeled external input with the pressure at the cone as the output. The poles are shifted by -100 on the real axis. Here the output pressure shown with the open loop output pressure, shows that the absorber reduced SPL peak levels around 100 Hz by 16 dB. The RMS sound pressure level, or SPL, dropped by 6 dB. It is also evident that some damping occured at the second acoustic resonance which was not intentionally designed around. Table 3.3 shows results of different pole locations for pressure feedback.

Matlab allows us to add infinite amounts of theoretical damping and gain results. However the voltage output limits the amount of damping that can be added in practice. A caveat to that statement is that when the experiment is ran, we can turn the output signal gain down to be a usuable signal. Infinite pole location, or

realistically moving the poles too far on the negative real axis, has its drawbacks in that moving them too far makes the resultant system have a higher static pressure level than the original system, thus making the overall SPL of the system increase. Thus, there are a range of values that provide the best damping.

Looking at the compensator in series with the plant, *KG(s)*, where *K(s)* is the compensator and *G(s)* is comprised of the transducer and tube according to Figure 3.13, is shown in Figure 3.14. This figure shows the sensitivity of the system where *KG(s)>1*, or the part of the response above 0 dB. Dorf and Bishop call this reducing the effect of the variation of parameters of the process (26). For these regions the controller is doing the bulk of the work and changes in the plant do not have a great impact on the system. Stability can also be inferred from this figure. This figure shows that we must use positive feedback if the system is to be stable. If negative feedback were to be used, the phase would be shifted down 180 degrees and then the line of interest is the -180 degree mark. Immediately we see that the system would be unstable at 100 Hz, so positive feedback must be used. It appears that only the peaks created by the coupling and the resonance at 200 Hz are above the 0 dB line. For this modeling case, it appears that we have enough control over the system to effectively add damping to the system. In the region of interest, namely between 80 Hz and 120 Hz, there is a 360 degree phase lag. As the compensator tries to move the poles further back to add more damping, this phase lag can seriously reduce the effectiveness of the control techniques and potentially cause an instability. The phase lag could cause instability if there are any errors in the model.

Figure 3.15a shows the results using displacement feedback. Here we have reduced the peak displacement levels, which corresponds to a reduction in pressure levels as evident in Figure 3.15b. Shown is for a pole location of -100 on the real axis. The resulting drop in pressure is 5.37 dB RMS and 17 dB peak. Table 3.4 shows the corresponding pressure reductions for different pole locations on the real axis. Comparing the compensator for displacement feedback in series with the plant, Figure 3.16 shows that similiar to using pressure as a sensor, the peaks are all above 0 dB. Thus, we are able to add damping to the peaks which corresponds to a reduction

Table 3.3: Modeled results using pressure feedback.

Real Part of Pole Location	RMS level (dB)	RMS Reduction (%)	Peak Reduction (dB)
no change	106.17	n/a	n/a
-30	104.71	15	10
-50	102.16	37	13
-100	100.01	50	16
-200	95.01	72	20

in sound levels inside the cavity. However, unlike pressure feedback, we do not have such a large phase lag, which may provide better control results and allow us to potentially add more damping to the system without causing an instability if errors in the model exist. This figure also shows that negative feedback is to be used.

In comparing the results, both methods of feedback produce reductions in sound levels within the tube as a result of an external excitation. The pressure feedback method seems to add more damping to the acoustic resonances than does the displacement feedback for the same pole locations. Comparing the compensator in series with the plant, *KG(s)* it is evident that the signal produced from displacement feedback allows us to have more control over the acoustics inside the tube. A major portion of the *KG(s)* for the pressure feedback lies below the 0 dB line, indicating that we may not be able to control the acoustics as much as we would like. There is a large phase lag in the region of interest which may hender or decrease the effects of the control law. This may be an important consideration when implementing the feedback controller.

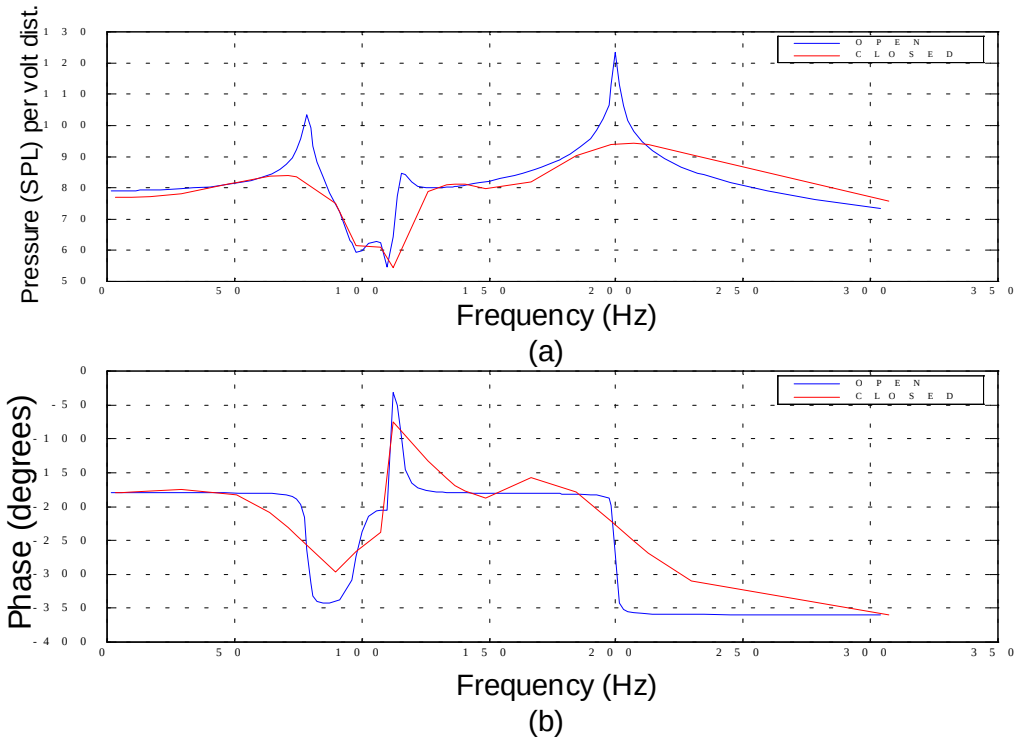

Figure 3.13: Closed loop results for pressure feedback: a) external input, pressure output, b) phase.

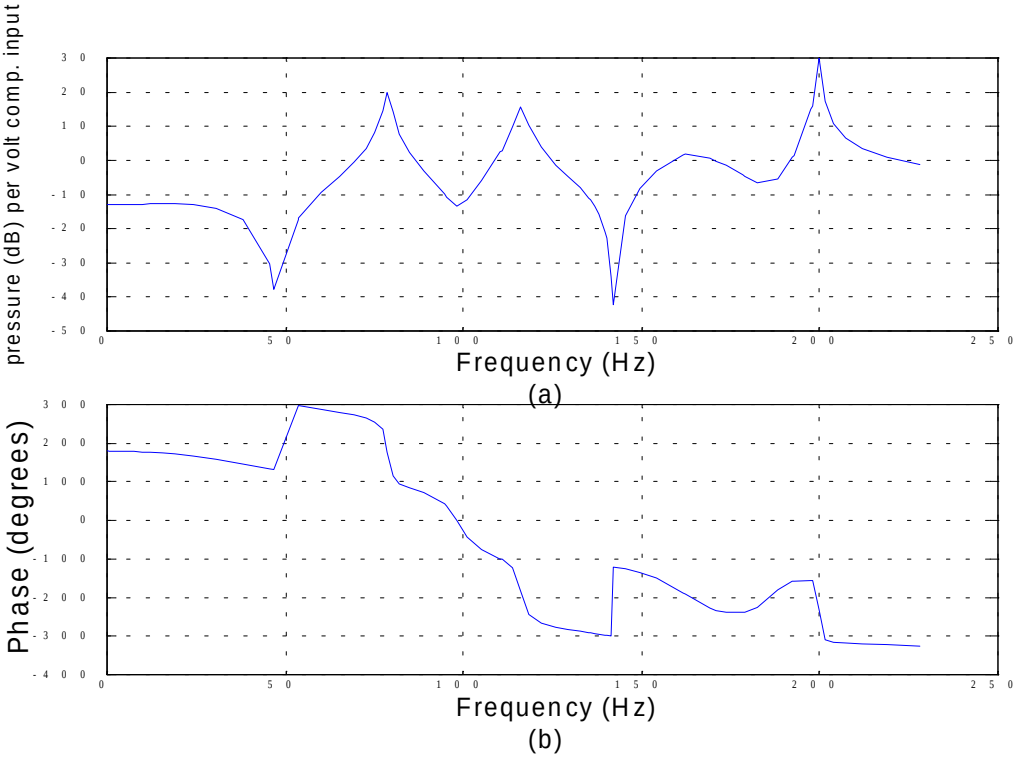

Figure 3.14: KG(s) for pressure feedback a) pressure per volt input b) phase.

Table 3.4: Modeled results using displacement feedback.

Real Part of Pole Location	RMS level (dB)	RMS Reduction (%)	Peak Reduction (dB)
no change	106.17	n/a	n/a
-30	104.06	21.5	10
-50	102.11	37	15
-100	100.8	46	17
-200	99.64	52.8	17

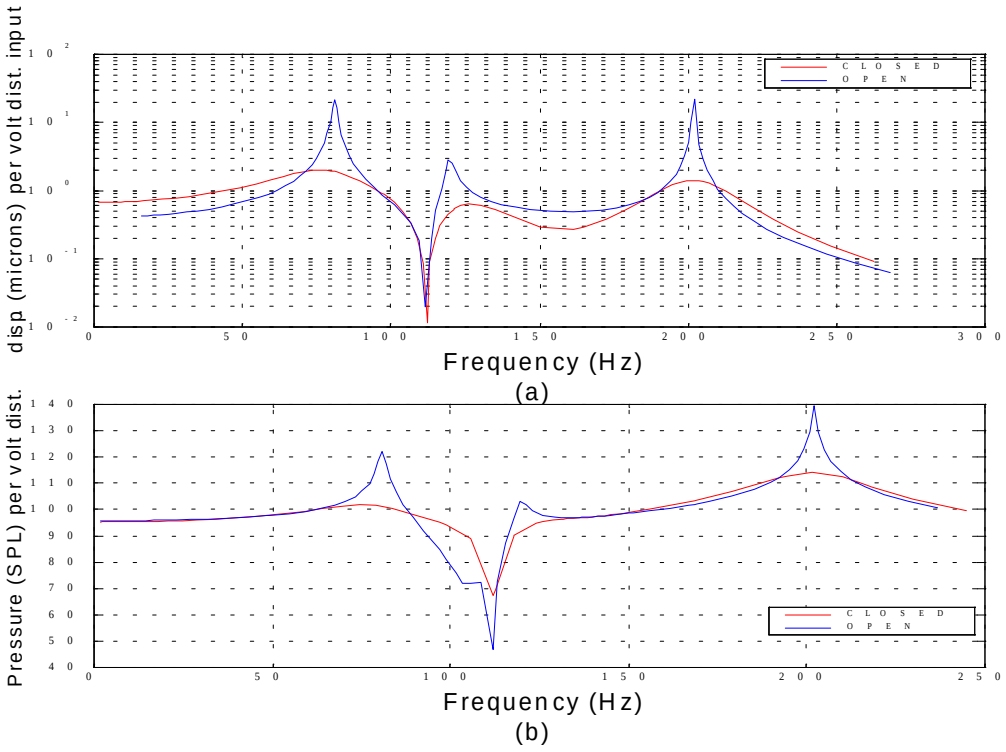

Figure 3.15: Closed loop results for displacement feedback: a) external input, displacement output, b) external input, pressure output.

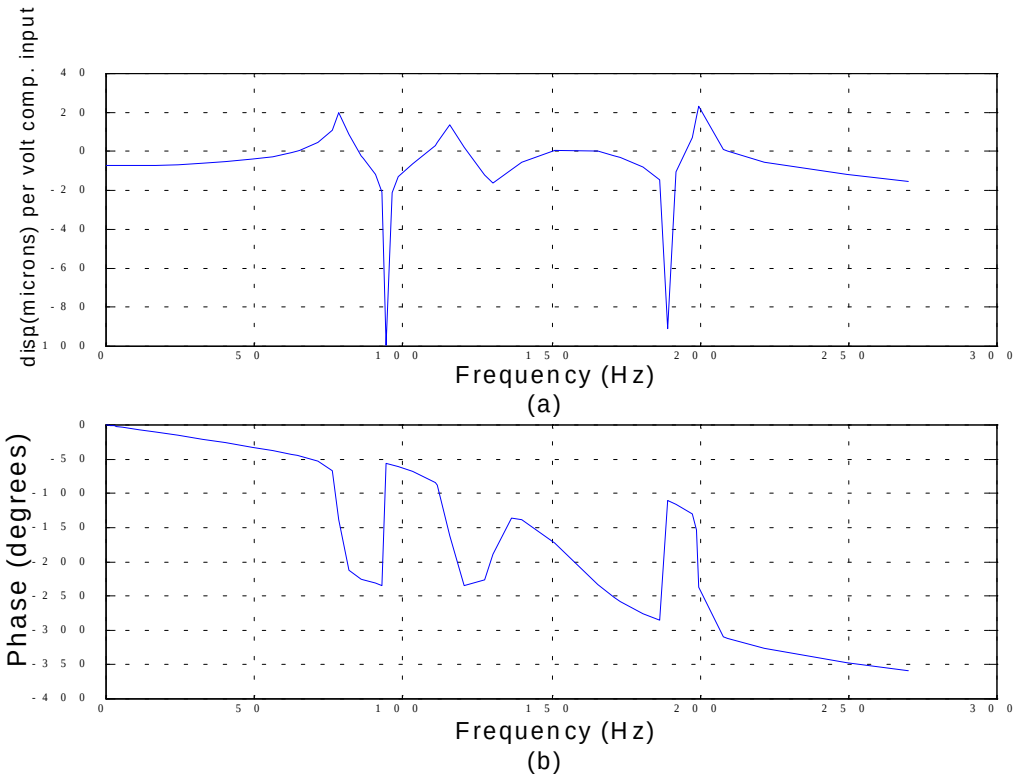

Figure 3.16: KG(s) for displacement feedback a) pressure per volt input b) phase.

Chapter 4

Transducer Design

4.1 Introduction

This chapter details the fabrication of the first generation piezoceramic transducer. Drawings used in the manufacture of the transducer are also displayed. It then discusses the construction phase and testing. Details of transducer dynamics and problems associated with the transducer are also discussed.

4.2 Design Concepts

As seen in Chapter 2, the concept behind the transducer entails using thin flexures actuated by piezoceramics to provide the stroke to an attached speaker cone. The entire transducer assembly consists of the flexures, actuators, cone, and housing. All parts are meant to be light weight which is the major advantage over using conventional electro-magnetic speaker for the active noise control driving element. However, in an early analysis using the unvalidated model, it appeared that the transducer would not give desired displacement.

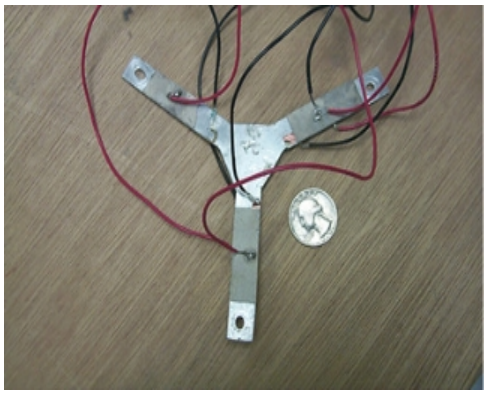

Figure 4.1: Actuation device for the first prototype transducer.

4.2.1 Initial Design

Construction of the first piezoceramic actuated transducer for this study was completed by Shannon Mauck. The design involved a beam structure that had three beams connected in the center. In the center of the structure, the cone was attached. This method proved to be unacceptable in that no appreciable amounts of displacement was provided. Turns out the structure was too thick and the center piece dramatically increased the stiffness of the actuation device. Figure 4.1 shows the actuation device for the first transducer. The design process then turned to the actuation device: redesigning the actuator to remove some stiffness and increase displacement.

Figure 4.2 shows the second transducer. This transducer utilized three individual beams as an actuation device. The three beams are attached to the voice coil of a cone taken from a conventional loudspeaker. This new transducer provided greater stroke at the flexures first resonance of 20 Hz, and provided the positive results to go ahead with that particular design.

4.2.2 Final Prototype Design

The wire frame version of the chosen transducer design is shown in Figure 4.3. The dimensions are taken from the modeled dimensions listed in Chapter 3. It consists of the three thin aluminum flexures which are 8.128 cm x 2.54 cm x 0.119 cm (3.2”

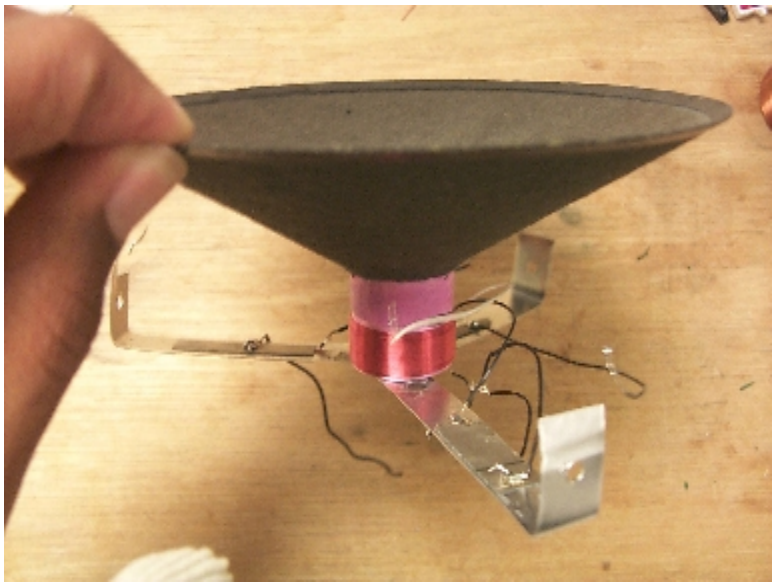

Figure 4.2: Cone and flexure assembly of second prototype piezoceramic transducer.

x 1" x 0.047"). The base of the beam, which is used to secure it to the housing, is 2.54 cm (1") long. The base is manufactured by bending the flexure in a clamp to a 90 degree angle with the plane of the surface of the beam. 0.3175 cm (1/8") holes are drilled into the tip of the beam and the support area, for connections to the cone and housing respectively. The beams weigh 14 grams each for a total of 42 grams. The control actuators are made of Piezo Systems 3.81 cm x 1.91 cm x 0.0254 cm (1 1/2" x .75" x 0.010") PZT-5A PZT piezoceramic patches attached on both sides of the flexures. The actuators are attached as a collocated pair. Figure 4.4 shows the rendered version of the design.

Upon completion of the individual flexures with attached piezoceramics, it is important that the beams are tested to ensure they have similiar characteristics, especially the first resonance. Using a PCB accelerometer, model number U352B22, attached with wax at the end of each beam, a transfer function using a Tektronix 2630 Fourier Analyzer to send a random signal to Trek HV Power Supply, Model 50/750 amplifier, to power the flexures, is generated. The results are shown in Figure 4.5. The first resonances of each beam are relatively close so we can be confident that the three beams have the same stiffness and mass values, thus we can multiply the mass

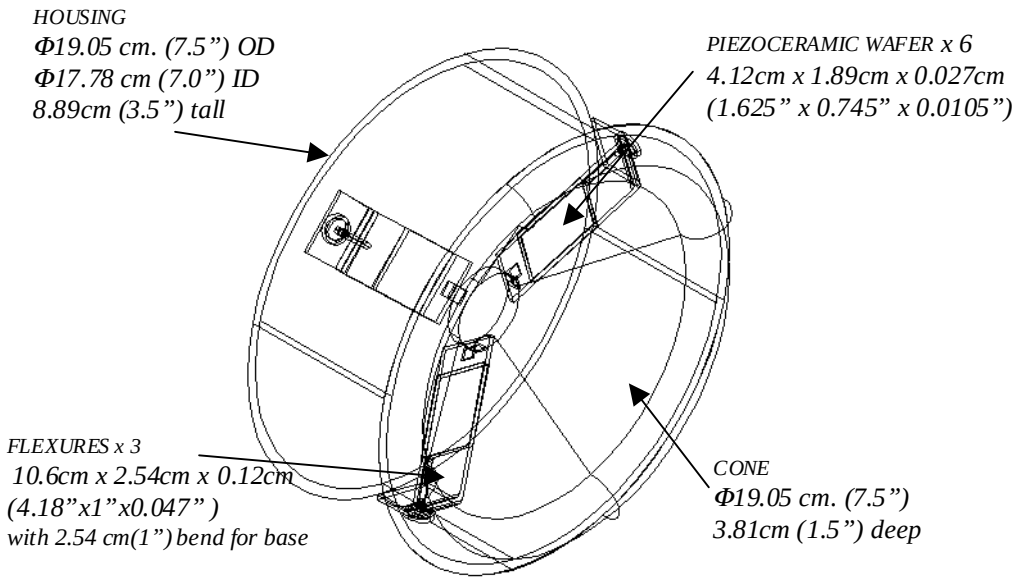

Figure 4.3: Wire frame view of transducer design.

matrix and stiffness matrices in the model by three to account for all three beams.

The speaker cone is taken from a 20.32 cm (8") Optimus Subwoofer. It is a paper cone coated with plastic for extra strength. The voice coil, which is attached to the cone and used in the conventional speaker setting, is trimmed down to 0.635 cm (1/4") from the base of the cone. This trimmed section of voice coil proved instrumental in attaching the cone to the flexures. Small holes are drilled into the voice coil at 120 degree increments. Thin aluminum elbows are constructed to secure the cone to the flexure.

The housing is constructed from a 15.24 cm (6") inner diameter PVC endcap for a 15.24 cm (6") PVC pipe. The round end of the end cap is removed leaving a cylinder of outer diameter 19.05 cm (7.5") which leaves a 1.27 cm (1/2") thick gap between the housing and the inner diameter of the tube. This gap is filled with a foam 0.635 cm (1/4") ring that is placed around the housing. Table 4.1 shows the weights of individual components in the transducer. Figure 4.6 shows the final assembly of

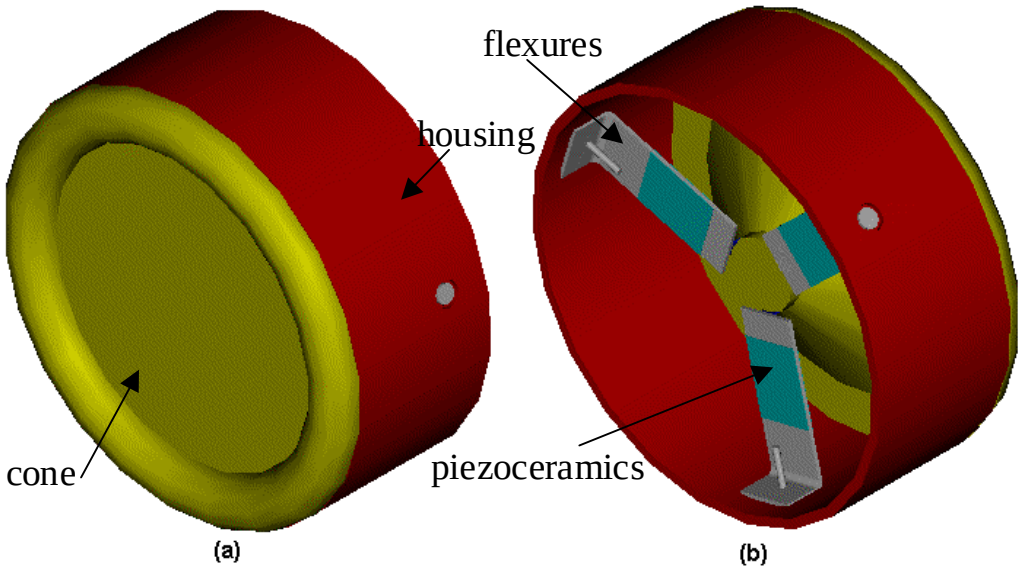

Figure 4.4: Rendered version of autocad drawing of transducer design: a) front view, b) rear view.

the parts.

4.3 Transducer Dynamics

Upon assembly of the transducer, testing is required to determine speaker dynamics. Using the Polytec OFV 040 scanning laser vibrometer aimed at the center of the cone, the transfer function of the transducer is taken with the Tektronix 2630 Fourier Analyzer. As discussed in Section 3.31, the combined speaker structural resonance is 100 Hz. This was the targeted resonance which will allow us to suppress noise levels at the first acoustic resonance of the tube. The static displacement, or the displacement associated with the flat portion of the transfer function, is 0.1 microns per volt. The piezoceramics can only take a safe applied load of roughly 100 volts, which is the limiting factor in this arrangement, giving a static displacement of 10 microns. At the resonance we can achieve approximately 150 microns of displacement.

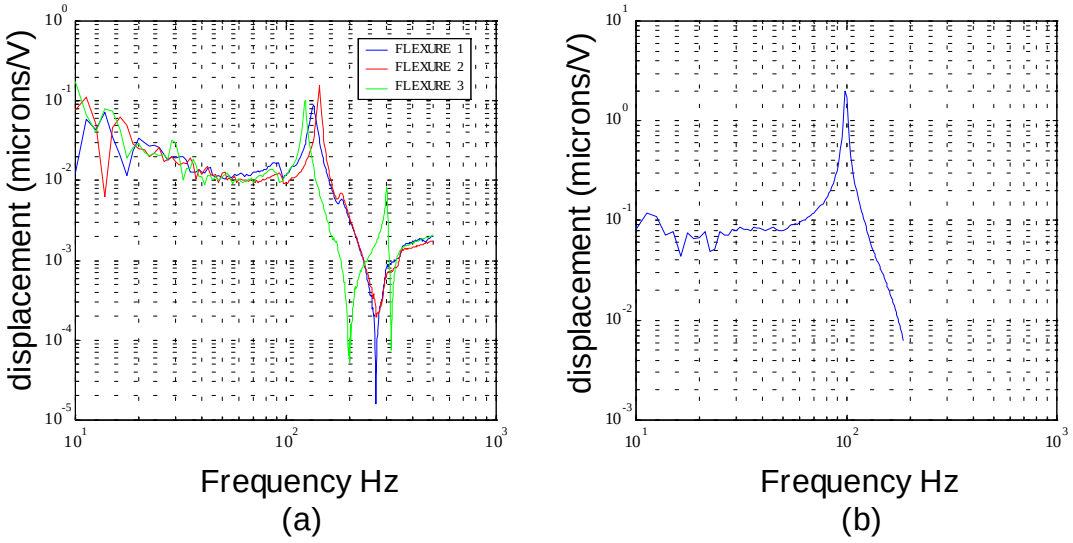

Figure 4.5: Testing of transducer dynamics: a) individual beam transfer functions, b) combined speaker dynamics.

Table 4.1: Individual weights of transducer components.

Component	Number of parts	Weight per part (grams)	Total Weight
flexures	3	14	42
elbows	3	0.6	1.8
piezoceramics	6	1.5	9
housing	1	562	562
foam ring	1	3	3
cone	1	21	21
fasteners	6	0.25	1.5
		TOTAL WEIGHT	640.3

Table 4.2: Summary of transducer characteristics.

Attribute	Value
natural frequency	100 Hz
static displacement	0.1 microns/V
peak displacement	1.5 microns/V
weight	0.64 kg
volume	2534 cm^3

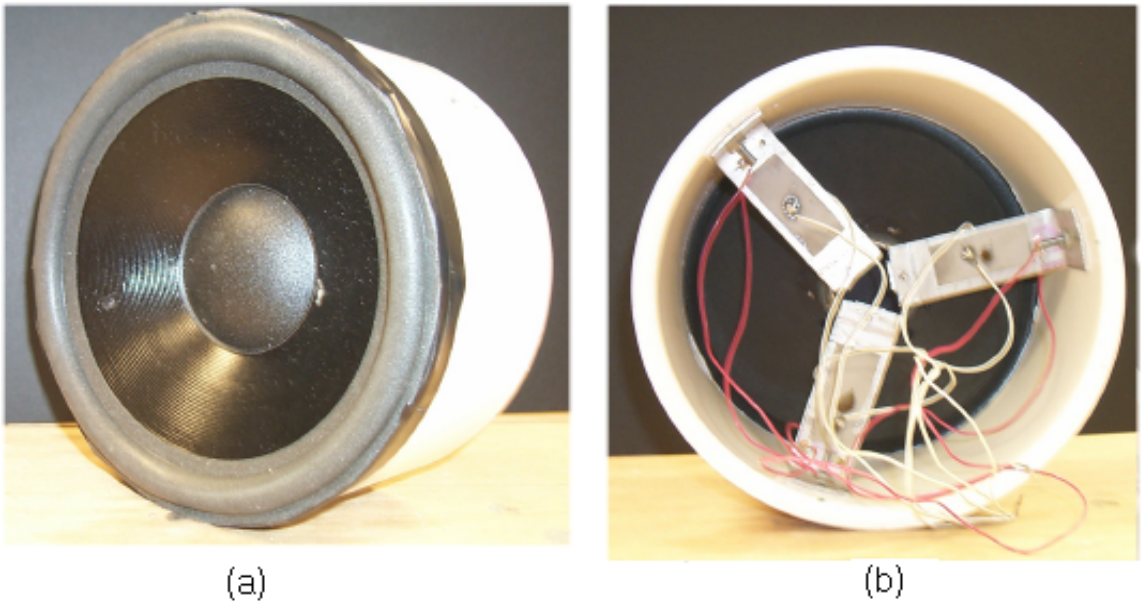

Figure 4.6: Completed Test Transducer: a) front view, b) rear view.

4.4 Problems With Transducer

As with any prototype, problems may exist. After prolonged use, it was noticed that the displacement of the transducer began to decrease, which was evident in decreased audible noise from the same magnitude input signal. It was found that the connections between the flexure and cone had worked themselves loose when faced with the continous random input to the piezoceramics. It was also found that the transducer contains inherent damping. We feel the connections may be part of it. Another possible addition of damping is the electrical tape that was used to secure the cone to the housing. In a test, a speaker transfer function was taken using the laser vibrometer with tape securing the cone to the housing and one with out tape. It was found that tape added very little damping to the cone.

Chapter 5

Experimental Results

In this chapter, we use the prototype piezoceramic transducer to first validate the open loop pressure and displacement results from Chapter 3. After validating the open loop results, the transducer is then used in conjunction with a digital controller and close loop results are measured.

5.1 Test Setup

Figures 3.1 shows the concept for the test setup. This concept was followed closely with the design of the actual setup. Figures 5.1, 5.2, and 5.3 show the test setup used in this study. The tube used is a 1.83 m (6') long, 20.32 cm (8") inner diameter, 21.59 cm (8.5") outer diameter, lexan plastic tube. As shown, the transducer is mounted on the end of the tube and sealed on the inside with the foam ring which fills the gap between the housing and the inner tube wall. The outside is encased by a special black tape that is placed on the tube and sealed around the outer wall of the transducer housing. It is particularly important to make sure no air leaks exist. Outside air acts as artificial damping to this case scenario and is not directly produced from the transducer setup, thus the time to seal the tube is important. Air also induces resonances that are not directly related to the motion of the transducer. On the opposite end, a wooden board is attached to the tube, also using the thick black tape. The wooden board was the second choice in termination material after it

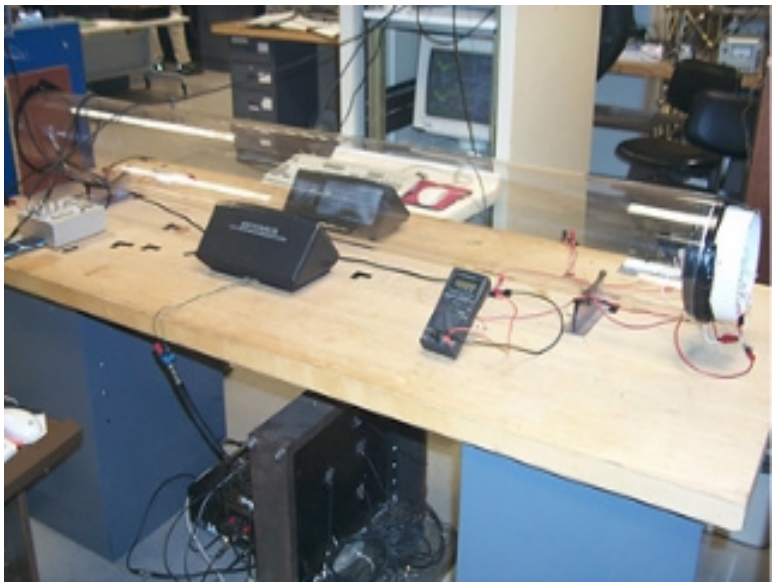

Figure 5.1: Side view of test stand.

was found that an end cap made of thin plastic enduced resonances from vibration felt from the external source. This study is focusing on the internal tube dynamics alone, and does not account for outside resonances.

Inside the tube are two Radio Shack omnidirectional electret microphones, part number 270-090C. One is mounted at the face of the transducer and the other is mounted at the opposite end of the tube. The connection wires are sent out through holes at the base of the tube and sealed with an epoxy. Mounted on the face of the transducer cone is a PCB Accelerometer, model number U352B22, attached with wax.

Two Optimus 3-way Bass Reflecting speakers are located in the center of the tube on both sides. These two loud speakers provide the external excitation used to stimulate the internal resonances by broadcasting white noise at the tube. Located between the two external speakers is a SPL meter, which provides the sound pressure level of the external source. A voltage meter is attached to the input leads of the transducer. This is a protective measure ensuring that the signal sent to the transducer does not damage the piezoceramics.

A Tektronix Fourier Analyzer is located nearby to measure frequency responses and generate the white noise signal used for the external excitation. Another com-

Figure 5.2: End view of test stand showing attached transducer.

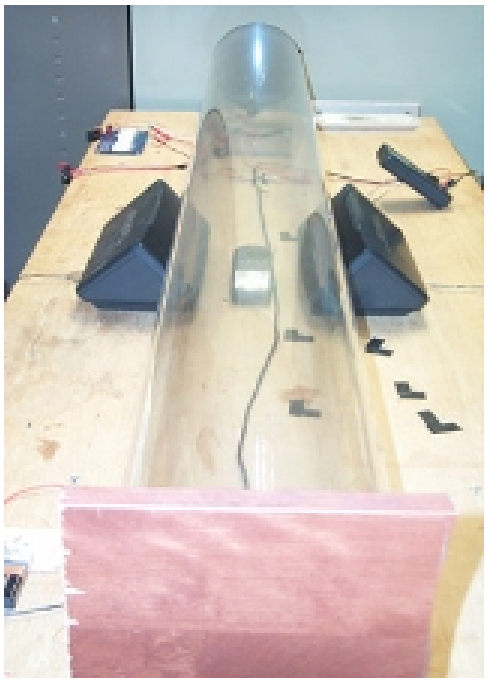

Figure 5.3: Top view of the test stand.

puter complete with Matlab v5.3 software, SIMULINK©, and a dSPACE DS1102 controller board with a TMS320C31 floating-point digital signal processor is used to generate and implement the digital controller. With this test setup, model validation and experimental results are taken.

5.2 Model Validation

Upon completion of the manufacturing of the prototype, the frequency response of the transducer was measured. Figure 5.4 shows the transducer experimental data with the modeled data of Chapter 3. The model fairly accurately models the motion of the transducer. However, -35 was added to the *A22* location in the transducer state-space model, shown below, which is the damping coefficent term, to match the experimental data is used throughout the study.

$$\begin{aligned} \dot{\bar{x}}_t &= \begin{bmatrix} 0 & 1 \\ A21 & -35 \end{bmatrix} \bar{x}_t + \begin{bmatrix} 0 & 0 \\ B21 & B22 \end{bmatrix} \bar{U} \\ y_t &= \begin{bmatrix} 1 & 0 \end{bmatrix} \bar{x}_t + \begin{bmatrix} 0 & 0 \end{bmatrix} \bar{U} \end{aligned}$$

Figure 5.5 shows the resulting tube pressure that is created by taking the transfer function between input voltage to the piezoceramics and the output pressure as seen by the microphone at the face of the transducer. The input voltage in Figure 5.5 is referenced to the input of the Trek amplifier which has a set gain of 20. Therefore, 1 volt out from the Tektronix is 20 volts into the piezoceramics of the transducer. The feedback modeling method fairly accurately predicts the coupling to the acoustic field inside the cavity. It does appear from the experimental data that the transducer/test setup contains damping at its first resonance. There is a small peak shown at 130 Hz in this experimental data. This particular set of experimental data was used to show how the acoustic dynamics of the tube vary with conditions, meaning that the tube has to be perfectly sealed. Shown in the experimental phase diagram, between 52

and 65 Hz, the phase jumps rapidly between -180 and 180. This is noise in the signal, which combined with the small peak at 130 Hz, may make it difficult to use microphones for pressure feedback. However, over all, the shape of the phase diagram and magnitude appear to reflect the experimental results. Therefore we can be confident that the state-space representation created accurately models the tube dynamics.

Figure 5.6 shows the resulting transducer displacement that is created by applying a voltage across the piezoceramics and measuring the displacement by a PCB accelerometer, model number U352B22. From the magnitude and phase plot, it is evident that there is more damping than the model contains. The transducer reflects the coupling with the first acoustic resonance as seen in the split peak. If these peaks were not evident in the cavity/transducer frequency response, then using displacement feedback techniques could not be applied. The first peak is off by 5 Hz. This will change the response of the closed loop response of the system if using displacement feedback because the observer will try to force the system to damp the modeled peak. If the compensator is robust enough, damping will still be added to the system. A better model of the cavity acoustics will be studied in future work.

5.3 Experimental Results Using Pressure Feedback

The initial feedback process involved using the microphone located at the face of the transducer cone as the feedback sensor. Realtime control was provided by a dSPACE DS1102 controller board with a TMS320C31 floating-point digital signal processor. The signal from microphone one is fed into the input one location of the DS1102 board. The input signal is sent through a filter to remove the DC gain associated with microphone signal conditioner. When using the Tektronix, it is easy to account for this DC offset by choosing the AC option under the input menu. However, the controller needs an input filter to filter out this DC gain and input strictly an AC signal. The signal is then converted to pressure by multiplying by the microphone calibration. The controller converts the input pressure into an output voltage that is fed into the leads to the the piezoceramics of the transducer. The complete SIMULINK© model

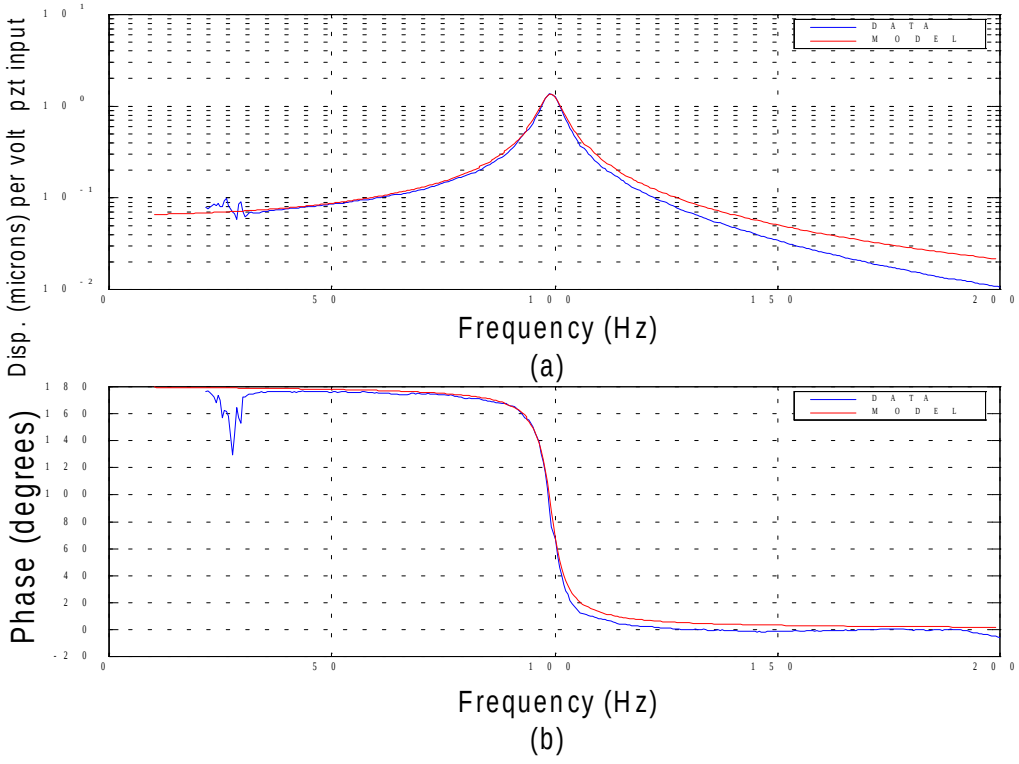

Figure 5.4: Validated transducer frequency response a) displacement b) phase.

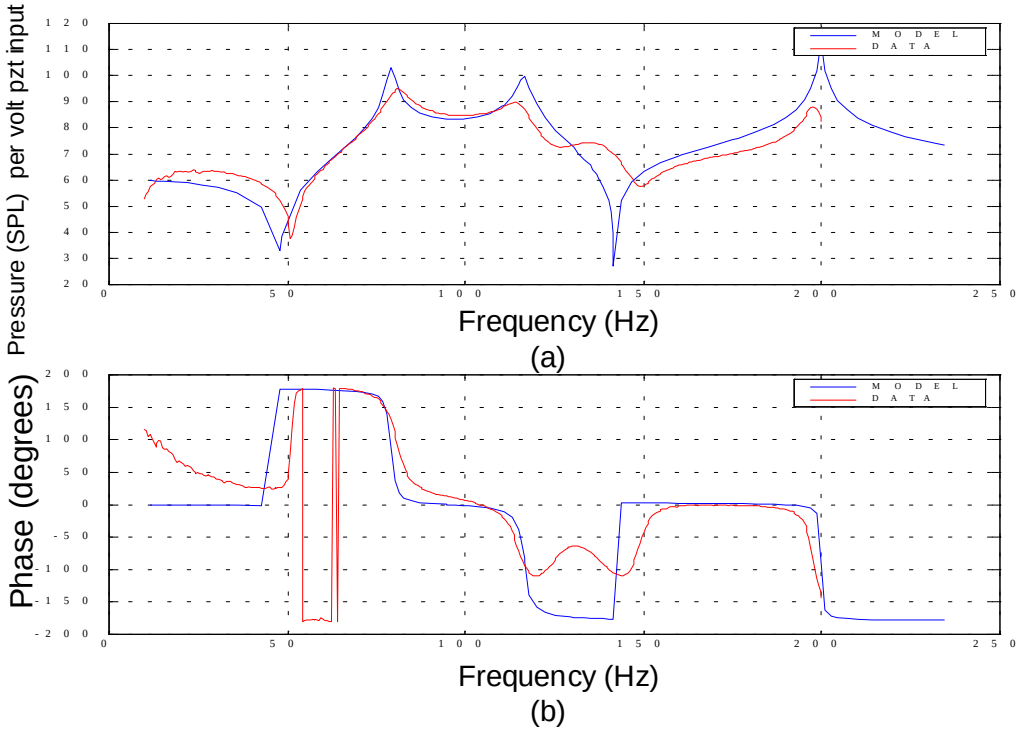

Figure 5.5: Validated cavity pressure frequency response a) sound pressure levels b) phase.

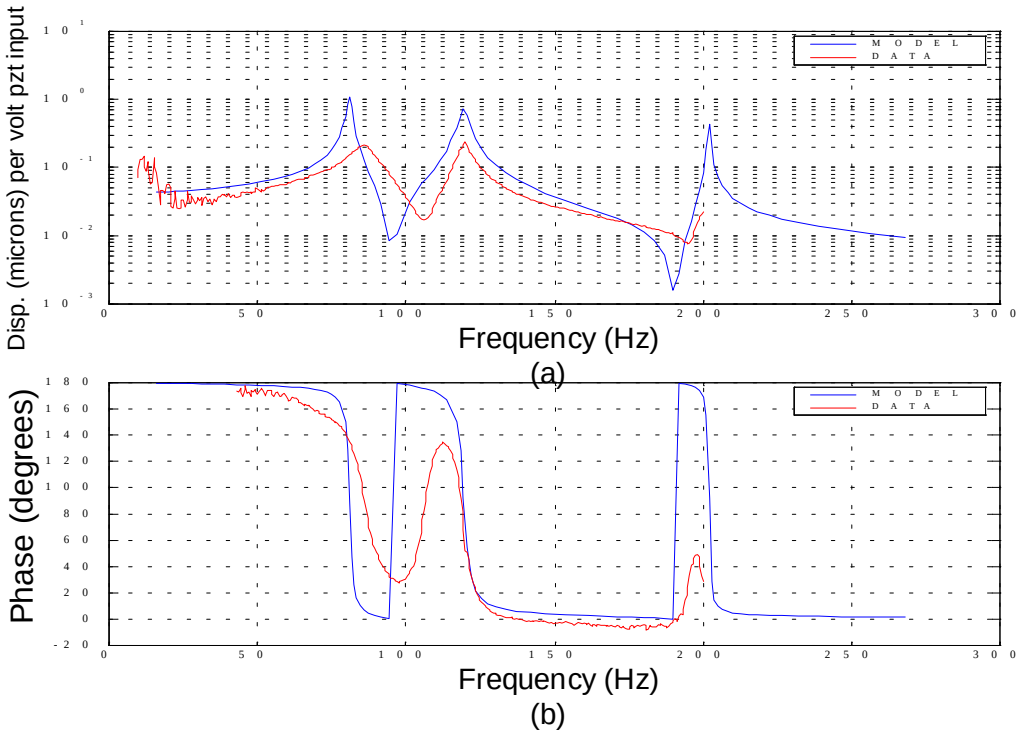

Figure 5.6: Validated transducer displacment attached to cavity a) displacement b) phase.

is included in Appendix E.

For this work, the external signal ranges from 0 to 200 Hz and all other calculations are based around this frequency range. Using 0 to 200 Hz for all calculations eliminates the need for anti-aliasing filters for unwanted frequency content that could possibly appear due to undersampling. The sample rate used is 0.002 seconds, for a sampling frequency of 5000 Hz.

In choosing poles, and thus adding damping to the system, the further the poles are moved, the higher the voltage levels seen at the output of the observer. However, this problem is easily rectified by adding a gain block at the output of the model that lowers the output voltage level. Figure 5.7 shows the results of using pressure feedback. The pressure is seen in SPL per volt of disturbance input, or input to the external loudspeaker from 0 to 200 Hz. As seen, there is virtually no damping added to the target resonance peaks, so the overall RMS pressure levels drop by only small margins. As the poles are moved further back on the real axis, it would be expected that the output signal would compensate and the pressure levels drop. This is not the case, which renders the pressure feedback as designed useless.

To see how the compensator is affecting the closed loop system, Figure 5.8 shows the *KG(s)* for the experimental pressure feedback. The units are volt per volt for the magnitude plot where the pressure is respresented as voltage from the microphone. From the magnitude plot, we see that the top portion of the two peaks that are intended to be controlled lie above the 0dB line. This indicates that we are able to add some damping to the system. However, using positive feedback as indicated by the model in Chapter 3, instabilities exist. Where the portion of the phase response crosses 0 degrees, the magnitude of *KG(s)* has to be less than 1 volt per volt, or 0 dB due to the denominator of a positive feedback system, *1 - KG(s)*. Again K is the compensator and G is the plant. Positive feedback indicates that KG is sensitive at 0 degrees on a phase diagram. If the magnitude of KG is equal or greater than 1 at 0 degrees, then the system will be unstable in the closed loop. Figure 5.8 shows that using positive feedback, at 120 Hz, the system is unstable. Using negative feedback, the magnitude at a phase of 180 degrees has to be less than -1 volt per

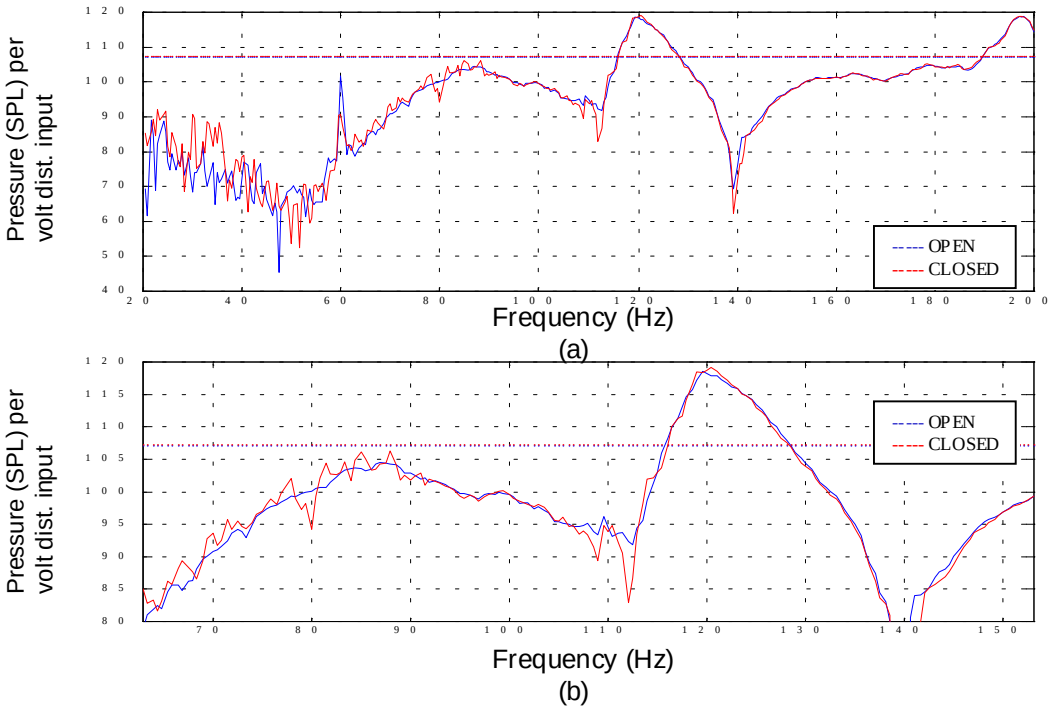

Figure 5.7: Typical result using pressure feedback a) sound pressure level, b) zoomed in around peaks.

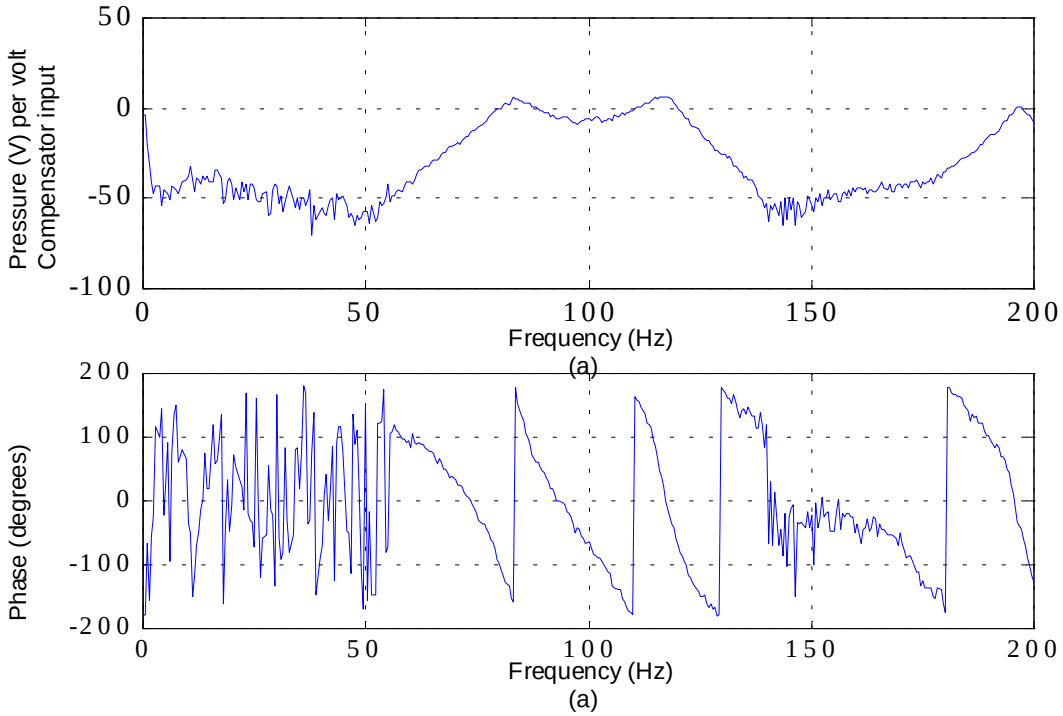

Figure 5.8: KG(s) for experimental pressure feedback a) magnitude, b) phase.

volt, or again 0 dB. Looking at figure 5.8, at 80 Hz, or the first peak, the system is unstable. Both negative and positive feedback contain instabilities, which indicates that the model has errors. Looking at positive feedback, it appears that we could add damping to the first peak and add negative damping or actually increase the sound level at the second peak. The same is true with negative feedback, the compensator can add damping to the second peak and increase levels at the first peak. This is due to the two peaks being out of phase from one another using pressure feedback.

The model has inherent errors that effect the system in a significant manner. It was assumed in the controller design that we had knowledge of all of the states. The states included displacement and velocity of the transducer and the pressure and its derivative for each acoustic resonance. The derivative of pressure has no significant meaning in this study, and is possible that the control gains generated based on the knowledge of these pressure derivatives negatively affects the controllability of the system. Also, as seen in Figure 5.5 there are some differences between the measured control signal and the theoretical model that may have impacted the overall effectiveness of the observer design. When the poles are moved further back on the negative real axis to add damping, the gain of the compensator increases and makes errors in the program propagate into the closed loop system. The actual SIMULINK© diagram could also be the problem in this design. If the incoming signal is not properly converted to a usuable input, the controller could output the wrong control signal. This pressure feedback method should be studied in future work to improve on the modeling techniques and controller design.

5.4 Experimental Results Using Displacement Feedback

After the absence of positive results using the pressure feedback method, displacement feedback was investigated as a means of introducing damping. In this method, the output matrices in the state-space model were modified to output the displacement

of the transducer, rather than the pressure seen at the face of the transducer. The PCB accelerometer, model number U352B22, was mounted on the cone to measure the acceleration of the cone. The signal is sent through a high-pass filter to eliminate any DC offset, and integrated twice digitally to input displacement to the observer. A sampling rate of 5 kHz is used to try to reduce the phase lag associated with the discretization of the observer. The output is again the control signal which is sent to the piezoceramics of the transducer. The SIMULINK© model is included in Appendix F.

Figure 5.9 shows the results of displacement feedback with progressively larger poles, or rather shifting the real part of the pole further on the negative side. The accelerometer was used for the feedback and the microphones were used to take the sound pressure results inside the tube. The results in Figure 5.9 display the damping achieved or not achieved with various pole locations. The results are seen as pressure inside the cavity, in SPL, per volt of input to the external source, which are the two loudspeakers mounted outside of the cavity. The signal from the Tektronix to the external loudspeakers is amplified 20x using an amplifier. The input SPL used is 104 dB. Tables 5.1 and 5.2 give the full results from the different pole locations and gains on the output signal for microphone one and two.

Figure 5.11 shows the *KG(s)* for displacement feedback. As seen in Figure 5.8, the *KG(s)* for pressure feedback, the top portion of the peaks we are adding damping to lie above the 0 dB line. More control is evident on the second peak due to more or the peak lying above the 0 dB line. This goes well with the results seen in Figure 5.9 and 5.10 because a greater peak reduction is noticed in the second peak. Using positive feedback, no instabilities exist and we can be confident that the compensator is working properly. Figure 5.11 has units of volt per volt where the output is from the accelerometer mounted on the cone in units of acceleration.

As seen in Figure 5.9 and 5.10, damping of the resonant peaks is achieved by moving the poles along the negative real axis. Figure 5.12 shows how the poles were moved. This study is on the feasibility of a piezoceramic transducer, so to keep the experiments relatively simple, only the real portion of the poles are moved.

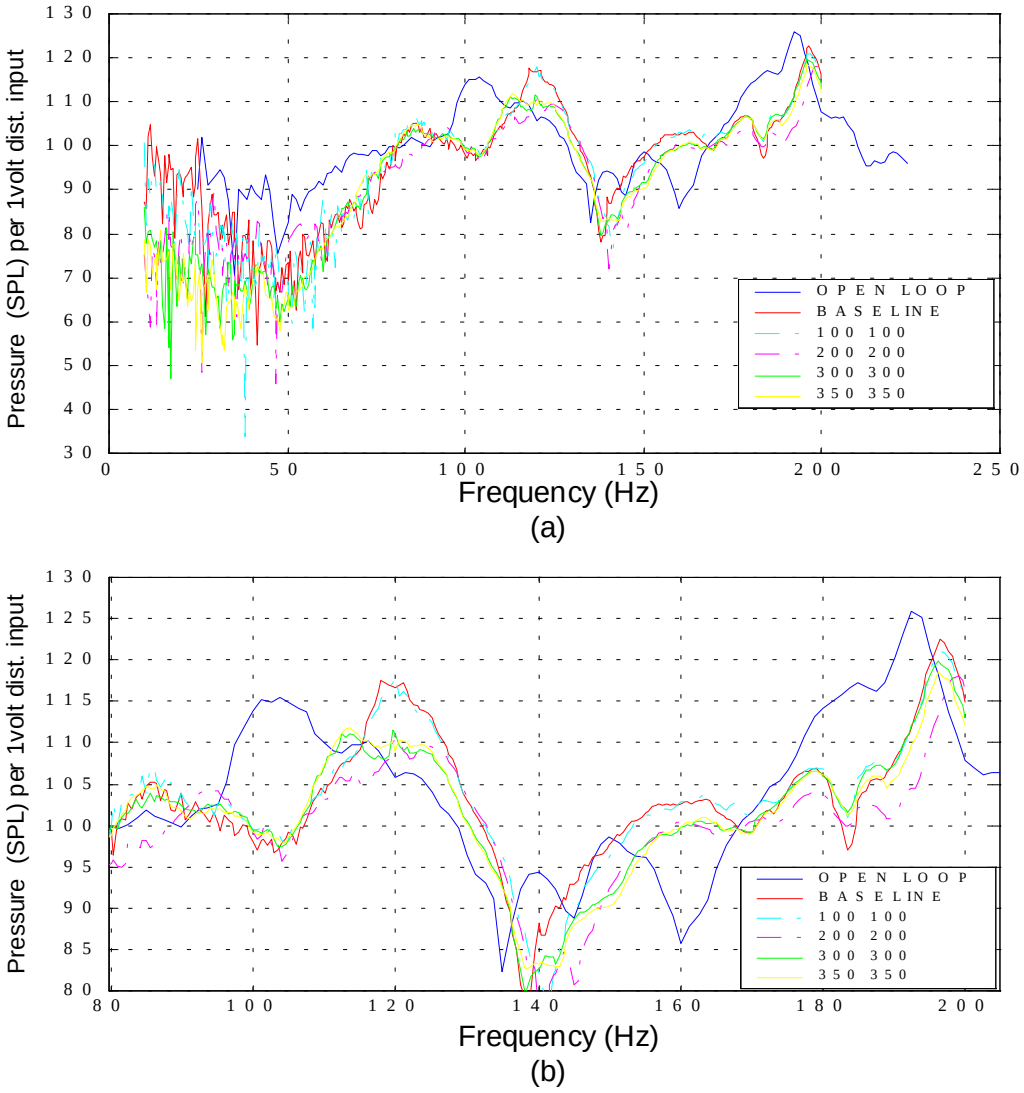

Figure 5.9: Results of various pole locations using displacement feedback for mic 1 a) frequency response up to 200 Hz b) zoomed in around target resonances.

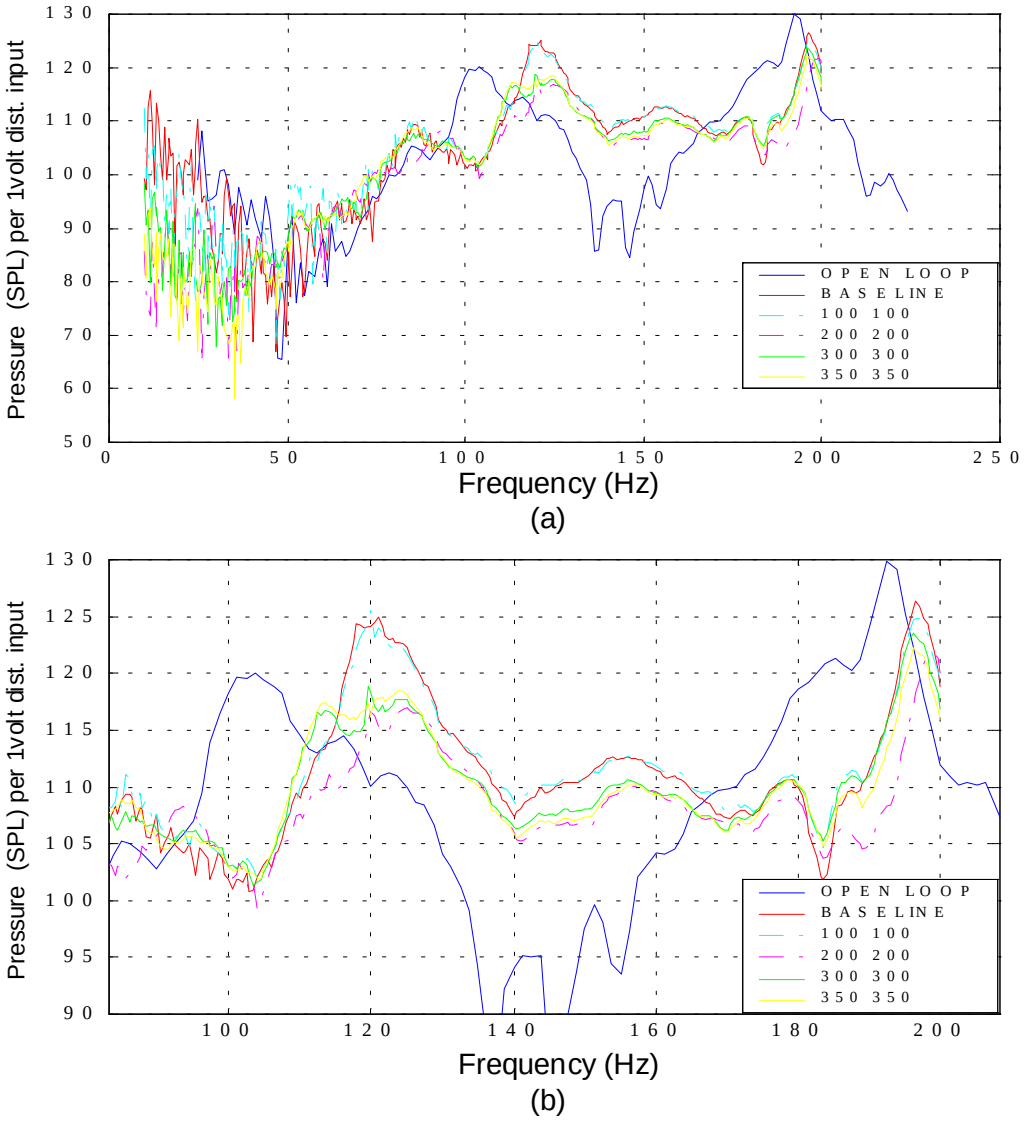

Figure 5.10: Results of various pole locations using displacement feedback for mic 2 a) frequency response up to 200 Hz b) zoomed in around target resonances.

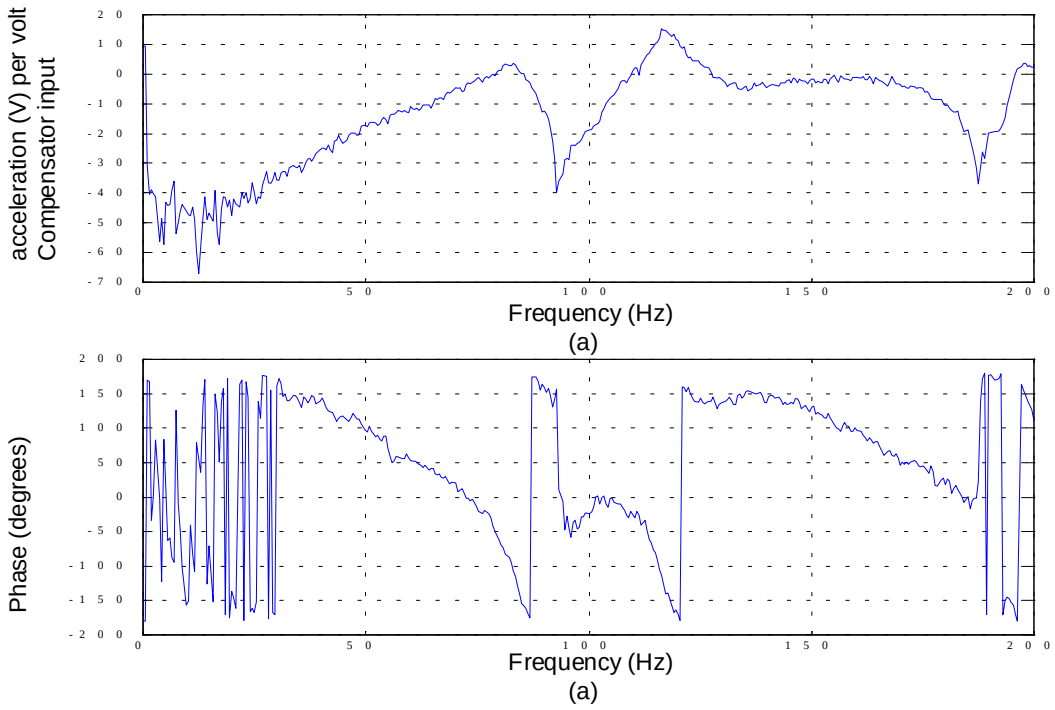

Figure 5.11: KG(s) for experimental displacement feedback a) magnitude, b) phase.

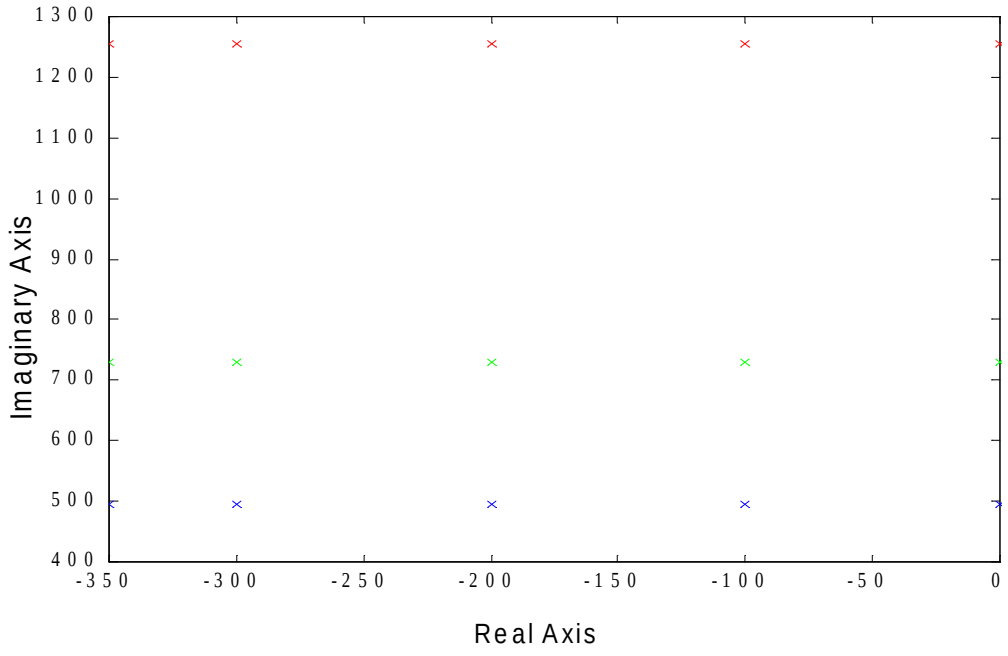

Figure 5.12: Plot of pole locations.

Damping occurs mainly in the higher sound level peak created by the coupling. It is also noticed that some damping occurs in the next acoustic resonance, 200 Hz, which was not the target resonance. No appreciable damping is noted in the next resonance of 300 Hz. Figure 5.9 shows the results at the face of the transducer. It was feared that the noise absorption would be localized to the area immediately around the transducer. Therefore a microphone was installed at the opposite end of the cavity. Figure 5.10 shows the results at the opposite end of the cavity. Sound pressure levels seem to increase over all for the open loop system, yet the transducer still provides adequate damping of the target resonances. Tables 5.1 and 5.2 give the numerical values of the reduction provided by each selected pole location. The case where both ends of the cavity are covered by rigid terminations is the *OPEN LOOP* case and is used to compare all other RMS results. The RMS sound levels are taken from 0 to 200 Hz. The *BASELINE* result in Figures 5.9 and 5.10 represents the transducer attached to the cavity with no control techniques applied. The *BASELINE* data is used for the comparison of peak reduction at 100 Hz. The peak reduction displays how much damping can be added by the transducer. Once the transducer is attached to the end of the cavity for control purposes, the sound pressure levels increase. This may be due to the fact that in the dual termination case, the wall is noncompliant, or has no motion, as a result of the external excitation. However, the transducer is in essence a flexible wall so when the tube is excited by the external source, the transducer is excited as well. This, is turn, produces a change in pressure that increases the over all internal pressure. The compliance of the transducer seems to have greater negative effects to the opposite end of the cavity where the sound pressure levels increase.

5.4.1 Observations

The limiting factor while using piezoceramics for this application is the amount of voltage the piezoceramics can recieve without producing an arc between the two contact leads or worse, simply burning the piezoceramic. Placing larger gains on the output signal of the digital controller, amplification of noise in the system occurs.

Table 5.1: Microphone 1 results from displacement feedback.

Real Part of Pole Location	Resulting RMS level	RMS Reduction (%)	Peak Reduction (dB)
dual endcap (baseline)	107.11	n/a	n/a
no change	107.85	8 (increase)	n/a
100 100	107.1	0.12	0.5
200 200	103.38	35	8
300 300	105.4	24.6	7
350 350	104.64	25	6

This may be due to increasing the compensator gain and thereby introducing an instability. Peaks that are relatively small compared to the targeted split peaks are amplified and create unwanted sound. Figure 5.13 shows the results of making the gain on the output signal larger than the intended output gain. Around the area of control, roughly 75 to 110 Hz, the figure with the high output gain has increased the sound pressure levels on peaks that are considered noise in the open loop system. Figure 5.13b shows the same amount of added damping but the original output from the controller. This figure has a smoother appearance and does not have any dramatic peaks.

In choosing the pole locations, the observer simply could not place the poles at a value of -375 and higher on the real axis. The output of the observer would simply be zero voltage accompanied with digital noise. Therefore this method of choosing poles is limited to -350 plus or minus the original imaginary axis value.

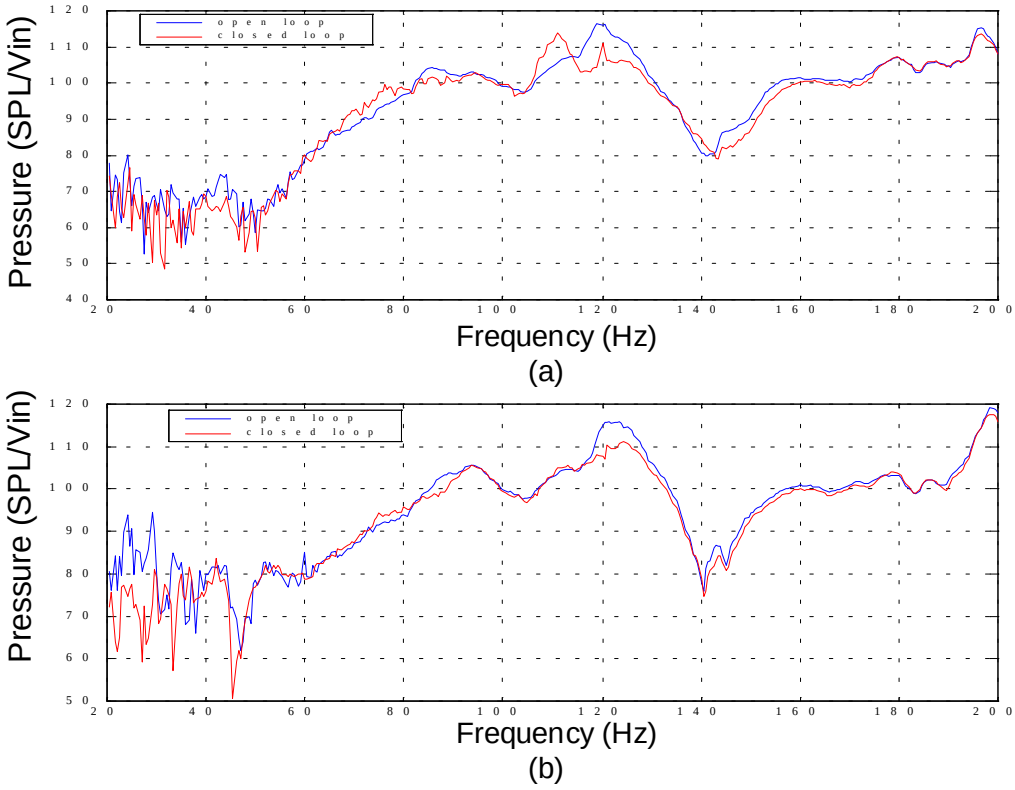

Figure 5.13: Results from experiment with pole locations moved to -200 on the real axis a)increased gain for more damping b)original gained signal from controller.

Table 5.2: Microphone 2 results from displacement feedback.

Real Part of Pole Location	Resulting RMS level	RMS Reduction (%)	Peak Reduction (dB)
dual endcap (baseline)	111.3	n/a	n/a
no change	113.87	25.6 (increase)	n/a
100 100	113.41	21.5 (increase)	1
200 200	108.91	30.8	9
300 300	110.79	2.3	7
350 350	110.37	5.7	8

Chapter 6

Conclusions and Future Work

6.1 Conclusions

A detailed analysis of the piezoceramic transducer model was studied for the purpose of interior noise control. A state-space representation was obtained of the transducer model which allowed several control law techniques to be studied. Transducer dimensions were determined from the model and applied to a final prototype design. The final prototype design came after a series of transducer designs and proved to be adequate. After attaching the transducer to the cavity, pressure feedback using a microphone mounted inside the cavity, was the initial parameter to be used in feedback, however, it proved to not give the desired results. Problems could have entailed a number of possibilties, which should be studied more closely. A second technique was used which utilized the displacement of the transducer which was measured by an accelerometer. This method produced results and allowed us to choose pole locations in order to add damping to desired acoustic resonances inside a six foot tube. The pole locations were not chosen in an optimal manner, but rather to prove that the transducer would in fact provide absorption.

From experimental results gathered using the prototype transducer with displacement feedback, the conclusion of this study is that a piezoceramic actuated transducer can be used in an active noise control solution as a driver element to achieve noise absorption. The findings suggest that although the displacement levels

produced by the 20.32 cm (8") transducer are on the micron scale, it will provide damping to target acoustic resonances inside a cylindrical cavity. Peak displacements are on the order of 200 microns, while the static displacement is on the order of 10 microns. The first acoustic resonance at 100 Hz is coupled by the transducer as evident in splitting into two individual peaks. These two peaks are reduced by 4 db and 8 db respectively for a total RMS reduction of 4 dB when using displacement feedback over a frequency range of 0 to 200 Hz. From the transfer function of the dual termination experiment, it is obvious there is some damping present at 100 Hz, which accounts for the rounded peak and lower reduction levels versus a completely non damped resonance. With the transducer attached to the cavity, sound pressure levels are noticed to increase, especially at the opposite end of the cavity. This is due to the compliance of the transducer and it creating more sound as a result of the movement of the cone. The transducer can not be used, as is, to affect multiple back to back resonances in this application due to the dynamics of the actuating device itself, in this case the beams. Thus, if the application necessitates the damping of four resonances, there would have to be a designated transducer per resonance, and multiples of the total target resonances to make up an acoustic array. However, noticeable peak reduction was seen in the second peak, namely a drop of 6 dB.

The prototype transducer weighs considerably less than an electromagetic loudspeaker at 0.64 kg, but still has room for improvement in the housing design. The housing for this study was for convenience rather than optimizing the weight, accounting for 87 percent of the 0.64 kg, but lighter plastic ares available which can produce the same results. This fact is promising in the aspect of using the piezoceramic actuated transducer for aerospace applications because although the need for more transducers to achieve a certain level of damping may exist, the combined total weight of say 10 or 15 transducers would still only compare to that of two or three conventional speakers. Table 6.1 is a summary of all results gathered from this study.

The piezoceramic actuated transducer is still in its beginning stages. This study proves that the concept does indeed work, however to make this application useful in a real life acoustic problem, a more in depth study must be done.

Table 6.1: Summary of results from piezoceramic actuated transducer study.

TRANSDUCER CHARACTERISTICS	
weight	0.64 kg
natural frequency	100 Hz
static displacement @ 100 V	10 microns
peak displacement @ 100 V	200 microns
PRESSURE FEEDBACK	
modeled RMS reduction	72%
modeled PEAK reduction	20 dB
experimental RMS	no reduction
experimental PEAK	no reduction
DISPLACEMENT FEEDBACK	
modeled RMS reduction	53%
modeled PEAK reduction	20 dB
experimental RMS reduction	35 %
experimental PEAK reduction	8 dB

6.2 Future Work

This section is devoted to future work that may further this application. One item that should be further studied is the transducer itself. To make the transducer lighter, explore other materials for the housing. Work has been done with shaping piezoceramics to obtain maximum control, this too could be applied to the beam theory behind the transducer. Pressure feedback for this transducer in theory should work, and the control techniques using such should be further studied. Another possible feedback method that would eliminate more elements in an acoustic array is using the dual nature of the piezoceramic to act as a sensor, and use the current or strain as a feedback method.

A half scale model of a full size payload fairing has been created and should used for the next phase of this study. A larger transducer could be designed, or implement the acoustic array which utilizes several transducers to provide broadband low frequency absorption.

A closer look at the nondimensionalization of parameters for better acoustic coupling to the system should also be studied. The better the system couples to the acoustic field, the greater the potential for noise absorption. A more in depth model of the transducer test setup should also be studied. The feedback method into a pole/zero model of the acoustics seems to work well. However, a better model of the external source may lead to a better observer model and thus a better control element for active noise control.

Bibliography

[1] G. Kahre. "Delta." *Proceedings of the NASA-Industry Conference on Launch Environments of ELV Payloads.* Elkridge, Maryland, pp. 145-188, 1990.

[2] K. Elliot. "Titan Vibroacoustics." *Proceedings of the NASA-Industry Conference on Launch Environments of ELV Payloads* Elkridge, Maryland, pp. 189-215, 1990.

[3] H. Himelblau,D. L. Kern, G. L. Davis. "Development of Cassini Acoustic Criteria Using Titan IV Flight Data." *Proceedings of the 38th Annual Technical Meeting of the Institute of Environmental Sciences.* Nashville, TN, pp. 307-331, 1992.

[4] T. F. Bergen and D. L. Kern. "Attenuation of the Cassini Spacecraft Vibroacoustic Environment." *Proceedings of the 42nd Annual Technical Meeting of the Institute of Environmental Sciences.* Orlando, Florida, May 12-17, 1996.

[5] J. S. Paine. *Dissipative Acoustic Arrays For Interior Noise Control in Payload Fairings.* Air Force. Monthly Status Report #5, 1999.

[6] J. S. Paine. *Dissipative Acoustic Arrays For Interior Noise Control in Payload Fairings.* Air Force. Monthly Status Report #5 parts C:E, 1999.

[7] C. R. Fuller and R.J. Silcos. *Active control of interior noise in model aircraft fuselages using piezoceramic actuators.* AIAA Journal, 30:2613-2617, 1992.

[8] S. Griffin, C. Hansen, and B. Cazzalato. *Feedback control of structurally radiated sound into enclosed spaces using structural sensing.* Submitted to the Journal of Acoustical Society of America.

[9] J. Levine. *History Of Underseas Cables.* http://hyperarchive.lcs.mit.edu/telecom-archives/archives/history/underseas.cables

[10] M. Colloms. *High Performance Loudspeakers.* Fifth Edition. John Wiley and Sons, Chichester, 1998.

[11] L. L. Beranek. *Acoustics.* McGraw-Hill Book Company, 1954.

[12] A. D. White. *On Loudspeaker Implementation for Feedback Control, Open-Air, Active Noise Reduction Headsets.* MS Thesis, Virginia Polytechnic Institute and State University, 1999.

[13] D. A. Bies and C. H. Hansen. *Engineering Noise Control.* Second Edition. Thompson Press, 1996.

[14] Piezo Systems, Inc. *A History of Piezoelectricity.* www.piezo.com ,1994.

[15] Z. Li. *Design of Active Structural Acoustic Control Systems Using Eigenassignment Approaches.* PhD Disseertation, Virginia Polytechnic Institute and State University, 1997.

[16] G. C. Smith. *Optimum Actuator Grouping in Feedforward Active Control Applications.* MS Thesis, Virginia Polytechnic Institute and State University, 1994.

[17] R. A. Burdisso and C. R. Fuller. "Theory of feedforward controlled system eigenproperties." *Journal of Sound and Vibration.* 153(3) pages 437-452, 1992.

[18] R. A. Burdisso and C. R. Fuller. "Dynamic behavior of structural-acoustic systems in feedforward control of sound radiation." *Journal of Acoustic Society of America.* 92(1) pages 277-286, 1992.

[19] W. R. Saunders, H. H. Robertshaw, and R. A. Burdisso. "An evaluation of feedback, adaptive feedforward and hybrid controller designs for active structural control of lightly-damped structure." *Proceedings of the 2nd Conference on Recent Advances in Active Control of Sound and Vibration.* Blacksburg, VA, pages 339-354, (Technomic Press, Lancaster, PA), 1993.

[20] C.C. Boucher, S. J. Elliot, and P. A. Nelson. "The effect of errors in the plant model on the performance of algorithms for adaptive feedforward control." *Special Issue of the Proceedings of Institution of Electrical Engineers.* 138 pages 313-319, 1991.

[21] S. M. Kuo and D. Vijayan. "Adaptive algorithms and experimental verification of feedback adaptive noise control systems." *Noise Control Engineering Journal.* 42(2) pages 37-46, 1994.

[22] Lueg Verfahren zur Dampfung von Schallsschwingungen. German Patent DRP No. 655 508.

[23] D. J. Inman. *Engineering Vibration.* Prentice-Hall, Englewood Cliffs, 1994.

[24] Piezo Systems, Inc. *Catalog # 3.* Cambridge, Massachusetts, 1998.

[25] D. J. Leo, K. W. Green, and S. Mauck. "Sound Absorbing Transducer For Interior Noise Control." *Proceedings of Active 99.* pg 1205 - 1214, 1999.

[26] R. C. Dorf and R. H. Bishop. *Modern Control Systems.* Eighth Edition. Addison-Wesley, Menlo Park, California, 1998.

[27] B. Friedland. *Control System Design-An Introduction to State-Space Methods.* McGraw-Hill, New York, New York, 1986.

Appendix A

MATLAB code for open loop analysis

```
%%%%%%%%%%%%%%%%%%%%%%%%%%%%%%%%%%%%%%%%%%%%%%%%%%%%%%%%%%%%%%%%%%%%%%%%%%%%
% K I M B A L L    G R E E N
% PROGRAM FOR MULTIPLE ACOUSTIC MODES AND MULTIPLE STRUCTURAL MODES OF
% A PIEZOCERAMIC SPEAKER WITH 3 FLEXURES AND A CONE.
%%%%%%%%%%%%%%%%%%%%%%%%%%%%%%%%%%%%%%%%%%%%%%%%%%%%%%%%%%%%%%%%%%%%%%%%%%%%


close all;clear all;
mo = input('Input the number of structural modes: ');
po = input('Input the number of acoustic modes: ');
L1=3.2; %length of beam in inches
x1=5/16; %distance to from tip of beam to pzt
L=L1*0.0254; %length of beam in meters
La1=(1.625); %length of pzt in inches
La=La1*0.0254; %length of pzt  in meters
x2=La1+x1; %distance from tip to end of pzt
hb=(0.047*0.0254); %height of aluminum cross section
b=(1)*0.0254; %base of aluminum cross section
wa=.745*0.0254; %width of pzt
ha=0.0105*0.0254; %height of pzt


%%%%%%%%%%%%%%%%%%%%%%%%%%%%%%%%%%%%%%%%%%%%%%%%%%%%%%%%%%%%%%%%%%%%%%%%%%%%
% Call for matrices that compute values based on number modes.
% with exception of BA which requires distance from tip to front of
% PZT and distance from tip to end PZT, and length of beam
%%%%%%%%%%%%%%%%%%%%%%%%%%%%%%%%%%%%%%%%%%%%%%%%%%%%%%%%%%%%%%%%%%%%%%%%%%%%
```

```
%chose 1 for clamped free boundary condition, 2 for clamped sliding boundary
[Mp]=mp_matrix(mo,L1,L1,1); %(modes,actual location of mass,length beam,boundary)
[Mb]=3*mb_matrix(mo,1); %(modes,boundary condition)
[BA]=(ba_matrix(mo,x1,x2,L1,1))';
%(modes,length to pzt, length to end pzt, length beam, boundary)
[Kb]=3*kb_matrix(mo,1); %(modes,boundary condition)
[BPP]=bp_matrix(mo,L1,L1,1); %(modes,actual location of mass,length beam,boundary)

BP=BPP';

%%%%%%%%%%%%%%%%%%%%%%%%%%%%%%%
%      CONSTANTS          %
%%%%%%%%%%%%%%%%%%%%%%%%%%%%%%%


Area=b*hb;    %area of aluminum cross section
palum=2.7e3;   %kg/m3 for aluminum density
mb=palum*Area*L; %mass of beam
mp=.021; %mass of piston in kilograms
mu=mp/(3*mb); %dimensionless parameter

modes = sprintf('modes: %2.0f       poles/zeros: %2.0f',mo,po)
mass = sprintf('mass of beam: %6.4f kgs        mass of piston: %6.4f kgs',mb,mp)


E=7.31e10; %N/m2  modulus for aluminum
I=(1/12)*b*hb^3; %moment of inertia for aluminum beam
d31=-320e-12; %piezoelectric strain coefficient for pzt
xo=d31*La/ha; %stress-free extension per unit volt
Y11=6.2e10; %elastic modulus
ka=wa*ha*Y11/La; %actuator stiffness
Ap=pi*(4*0.0254)^2; %area of piston
pair=1.16; %kg/m3 for air-density
c=343; %speed of sound in air m/s2
l=5.95*12*0.0254; %length of tube


%%%%%%%%%%%%%%%%%%%%%%%%%%%%%%%%%%%%%%%%%%%%%%%%%%%%%%%%%%%%%%%%%%%%%%%%%%%%
%BUILDING OF STRUCTURAL MODE STATE SPACE MODEL
%%%%%%%%%%%%%%%%%%%%%%%%%%%%%%%%%%%%%%%%%%%%%%%%%%%%%%%%%%%%%%%%%%%%%%%%%%%%

a=Ap*BP'*(pair*c^2)/(Ap*l); %grouping some terms
M=(Mb+mu*Mp); %grouping mass terms

%GROUPED TERMS IN A MATRIX
A21=-((M^-1*(E*I/(mb*L^3))*Kb)+(M^-1*(1/(mb*L))*(BA)*(ka*(hb+ha)^2)*(BA)'));
```

```
%GROUPED TERMS IN B MATRIX
B21=M^-1*(1/(mb*L))*(BA)*(xo*ka*(hb+ha));
B22=(-(M^-1*Ap*(1/mb)*BP));

%NONDIMENSIONAL PARAMETERS
kappaa=(6*E*L *(1+hb/ha)^2)/(Y11*La*(hb/ha)^3);
kappat=(pair*c^2*Ap*L^3)/(E*I*l);
mu;

dimen = sprintf('Ka:  %6.3f   Kt: %6.3f   mu: %6.3f',kappaa,kappat,mu)


%DEFINING STATE SPACE MODEL
if mo >1
A=[zeros(mo,mo),eye(mo);A21,zeros(mo,mo)];
else
A=[0,1;A21,-35];
end


B = [zeros(mo,1) zeros(mo,1);B21 B22];
C = [BP' zeros(1,mo)];
D = [0 0];


syss1=ss(A,B,C,D);

w = logspace(1,3,1000)*2*pi;

[mag1,pha1,w1]=bode(A,B,C,D,1,w);

%%%%%%%%%%%%%%%%%%%%%%%%%%%%%%%%%%%%%%%%%%%%%%%%%%%%%%%%%%%%%%%%%%%%%%%
%Plots the transducer displacement and phase
%%%%%%%%%%%%%%%%%%%%%%%%%%%%%%%%%%%%%%%%%%%%%%%%%%%%%%%%%%%%%%%%%%%%%%%

figure
load laser100
loglog(FreqV(21:401),abs(Xfer31(21:401))),grid
hold on
loglog(w1(1:650)/2/pi,mag1(1:650)/1e-6,'R')
legend('data','model')
grid

figure
rad2 = atan2(imag(Xfer31),real(Xfer31));deg2 = 180*rad2./pi;
semilogx(FreqV(21:401),deg2(21:401),'B'),grid
```

```
hold on
semilogx(w1(1:650)/2/pi,pha1(1:650),'R')
grid

%%%%%%%%%%%%%%%%%%%%%%%%%%%%%%%%%%%%%%%%%%%%%%%%%%%%%%%%%%%%%%%%%%%%%%%%%%%%
% P R E S S U R E    T E R M S
%%%%%%%%%%%%%%%%%%%%%%%%%%%%%%%%%%%%%%%%%%%%%%%%%%%%%%%%%%%%%%%%%%%%%%%%%%%%


for i = 1:po
wp(i) = i*pi*c/l;
wz(i) = (2*i-1)*pi*c/(2*l);
end

num = [1 0 wz(1)^2];
den = [1 0 wp(1)^2];

for i = 1:po-1
num = conv(num,[1 0 wz(i+1)^2]);
end

anot = (pair*c^2)/(l);
numm = anot*num;


for i = 1:po-1
den = conv(den,[1 0 wp(i+1)^2]);
end

w = logspace(1,3,1000)*2*pi;

[AaA,BbB,CcC,DdD]=tf2ss(numm,den);%creates state-space model from tf
press=ss(AaA,BbB,CcC,DdD);


%%%%%%%%%%%%%%%%%%%%%%%%%%%%%%%%%%%%%%%%%%%%%%%%%%%%%%%%%%%%%%%%%%%%%%%%%%%%
%creates feedback of pressure from tube to transducer
%%%%%%%%%%%%%%%%%%%%%%%%%%%%%%%%%%%%%%%%%%%%%%%%%%%%%%%%%%%%%%%%%%%%%%%%%%%%

system= feedback(syss1,press,2,1,+1);%positive feedback due to
%impedance model having
%negative sign at low frequencies
w = logspace(1,3,1000)*2*pi;
[Aa,Bb,Cc,Dd]=ssdata(system);

S=[DdD*C CcC];  %outputs total pressure from over all system
```

```
%%%%%%%%%%%%%%%%%%%%%%%%%%%%%%%%%%%%%%%%%%%%%%%%%%%%%%%%%%%%%%%%%%%%%%%
%PLOTS OPEN LOOP SYSTEM SIMULATING FEEDBACK FROM MICROPHONE
%COMPARES MICROPHONE OUTPUT TO SIMULATED PRESSURE OUTPUT
%%%%%%%%%%%%%%%%%%%%%%%%%%%%%%%%%%%%%%%%%%%%%%%%%%%%%%%%%%%%%%%%%%%%%%%

figure
[magP1,phaP1,w]=bode(Aa,Bb,S,Dd);
semilogx(w(13:100)/2/pi,20*log10(magP1(13:100,1)/(.15*sqrt(2)*20e-6)));
hold on
load pztube200
plot(FreqV(21:401),20*log10(abs(Xfer41(21:401)*0.1/(0.000562*20e-6))),'R')
legend('model','data')
grid

figure
[magP1,phaP1,w]=bode(Aa,Bb,S,Dd);
semilogx(w(13:100)/2/pi,phaP1(13:100,1),'B');
hold on
load pztube200
rad1 = atan2(imag(Xfer41),real(Xfer41));deg1 = 180*rad1./pi;
plot(FreqV(21:401),deg1(21:401),'Y')
grid
figure
legend('model','data')

%%%%%%%%%%%%%%%%%%%%%%%%%%%%%%%%%%%%%%%%%%%%%%%%%%%%%%%%%%%%%%%%%%%%%%%
%PLOTS OPEN LOOP SYSTEM SIMULATING FEEDBACK FROM ACCELEROMETER
%COMPARES DISPLACEMENT OUTPUT TO SIMULATED DISPLACEMENT OUTPUT
%%%%%%%%%%%%%%%%%%%%%%%%%%%%%%%%%%%%%%%%%%%%%%%%%%%%%%%%%%%%%%%%%%%%%%%



q=(1:100);
figure
[magext,phaext,w]=bode(Aa,Bb(:,1),Cc,Dext(:,1));
semilogx(w(q)/2/pi,(abs(magext(q))/1e-6),'B');
grid
hold on
load aceltube
semilogx(FreqV(20:401),abs(Xfer31(20:401)*(-5.2e7)./(2*pi*FreqV(20:401)).^2))

q=(1:100);
figure
semilogx(w(q)/2/pi,phaext(q,1),'B')
hold on
rad2 = atan2(imag(Xfer31),real(Xfer31));deg2 = 180*rad2./pi;
```

```
semilogx(FreqV(87:401),deg2(87:401),'B'),grid
```

Appendix B

MATLAB code for validating the beam dynamics

```
%%%%%%%%%%%%%%%%%%%%%%%%%%%%%%%%%%%%%%%%%%%%%%%%
%Kimball Green
%beamvalid.m code to model beam dynamics
%%%%%%%%%%%%%%%%%%%%%%%%%%%%%%%%%%%%%%%%%%%%%%%%

mo=4;
L1=3.01; %length of beam in inches
x1=1.25; %distance to from tip of beam to pzt
L=L1*0.0254; %length of beam in meters
La1=(1.625); %length of pzt in inches
La=La1*0.0254; %length of pzt  in meters
x2=La1+x1; %distance from tip to end of pzt
hb=(0.03*0.0254); %height of aluminum cross section
b=(7/8)*0.0254; %base of aluminum cross section
wa=.75*0.0254; %width of pzt
ha=0.0105*0.0254; %height of pzt
mp=0.00005; %mass of piston in kilograms


%chose 1 for clamped free, 2 for clamped sliding
[Mp]=mp_matrix(mo,L1,L1,1); %(modes,actual location of mass,length beam,boundary)
[Mb]=mb_matrix(mo,1); %(modes,boundary condition)
[BA]=(ba_matrix(mo,x1,x2,L1,1))';
%(modes,length to pzt, length to end pzt, length beam, boundary)
[Kb]=kb_matrix(mo,1); %(modes,boundary condition)
[BPP]=bp_matrix(mo,L1,L1,1); %(modes,actual location of mass,length beam,boundary)

BP=BPP';

%%%%%%%%%%%%%%%%%%%%%%%%%%%%%%%
%      CONSTANTS
%%%%%%%%%%%%%%%%%%%%%%%%%%%%%%%
```

```
Area=b*hb;  %area of aluminum cross section
palum=2.7e3; %kg/m3 for aluminum density
mb=palum*Area*L;
mu=mp/mb; %dimensionless parameter

E=7.31e10; %N/m2  modulus for aluminum
I=(1/12)*b*hb^3; %moment of inertia for aluminum beam
d31=-320e-12; %piezoelectric strain coefficient for pzt
xo=d31*La/ha; %stress-free extension per unit volt
Y11=6.2e10; %elastic modulus
ka=wa*ha*Y11/La; %actuator stiffness

%%%%%%%%%%%%%%%%%%%%%%%%%%%%%%%%%%%%%%%%%%%%%%%%%%%%%%%%%%%%%%%%%%%%%%%%%%%
%BUILDING OF STRUCTURAL MODE STATE SPACE MODEL
%%%%%%%%%%%%%%%%%%%%%%%%%%%%%%%%%%%%%%%%%%%%%%%%%%%%%%%%%%%%%%%%%%%%%%%%%%%

M=(Mb+mu*Mp); %grouping mass terms

%GROUPED TERMS IN A MATRIX
A21=-((M^-1*(E*I/(mb*L^3))*Kb)+(M^-1*(1/(mb*L))*(BA)*(ka*(hb+ha)^2)*(BA)'));

%GROUPED TERMS IN B MATRIX
%B21=[zeros(mo,1)];
B21=M^-1*(1/(mb*L))*(BA)*(xo*ka*(hb+ha)); %assumes 1 volt in
%102325 for 1 pascal above atmospheric


%DEFINING STATE SPACE MODEL
if mo >1
A=[zeros(mo,mo),eye(mo);A21,[-50 0 0 0;0 -45 0 0;0 0 -45 0;0 0 0 -45]];
else
A=[0,1;A21,-35];
end

B = [zeros(mo,1);B21];
C = [BP' zeros(1,mo)];
D = [0];


syss1=ss(A,B,C,D);

[mag1,pha1,w1]=bode(A,B,C,D);

close all
```

```
figure
load bare5k2
loglog(FreqV(3:401),abs(Xfer31(3:401)*(-5.2e7)./(2*pi*FreqV(3:401)).^2))
hold on
loglog(w1/2/pi,mag1/1e-6,'R')
legend('data','model')


figure
load load5k2
loglog(FreqV(3:401),abs(Xfer31(3:401)*(-5.2e7)./(2*pi*FreqV(3:401)).^2))
hold on
loglog(w1(1:102)/2/pi,mag1(1:102)/1e-6,'R')


figure
load wash5k
loglog(FreqV(4:401),abs(Xfer31(4:401)*(-5.2e7)./(2*pi*FreqV(4:401)).^2))
hold on
loglog(w1(1:102)/2/pi,mag1(1:102)/1e-6,'R')
legend('data','model')
hold on
load wash100
loglog(FreqV(15:150),abs(Xfer31(15:150)*(-5.2e7)./(2*pi*FreqV(15:150)).^2))
```

Appendix C

MATLAB code for simulating the closed loop response

```
%%%%%%%%%%%%%%%%%%%%%%%%%%%%%%%%%%%%%%%%%%%%%%%%%%%%%%%%%%%%%%%%%%%%%%%%
% K I M B A L L    G R E E N
% PROGRAM FOR MULTIPLE ACOUSTIC MODES AND MULTIPLE STRUCTURAL MODES OF
% A PIEZOCERAMIC SPEAKER WITH 3 FLEXURES AND A CONE.
%%%%%%%%%%%%%%%%%%%%%%%%%%%%%%%%%%%%%%%%%%%%%%%%%%%%%%%%%%%%%%%%%%%%%%%%


close all;clear all;
mo = input('Input the number of structural modes: ');
po = input('Input the number of acoustic modes: ');
gain = input('Input the amount of damping for full: ');
gain2 = input('Input the amount of damping for observer: ');



L1=3.2; %length of beam in inches
x1=5/16; %distance to from tip of beam to pzt
L=L1*0.0254; %length of beam in meters
La1=(1.625); %length of pzt in inches
La=La1*0.0254; %length of pzt  in meters
x2=La1+x1; %distance from tip to end of pzt
hb=(0.047*0.0254); %height of aluminum cross section
b=(1.)*0.0254; %base of aluminum cross section
wa=.745*0.0254; %width of pzt
ha=0.0105*0.0254; %height of pzt
radius=4;

%%%%%%%%%%%%%%%%%%%%%%%%%%%%%%%%%%%%%%%%%%%%%%%%%%%%%%%%%%%%%%%%%%%%%%%%
% Call for matrices that compute values based on number modes.
% with exception of BA which requires distance from tip to front of
% PZT and distance from tip to end PZT, and length of beam
%%%%%%%%%%%%%%%%%%%%%%%%%%%%%%%%%%%%%%%%%%%%%%%%%%%%%%%%%%%%%%%%%%%%%%%%
```

```
%#function mp_matrix(x),mb_matrix(y),ba_matrix(x1,x2,x3,x4),
%kbbb_matrix(x),bp_matrix(x)

%chose 1 for clamped free, 2 for clamped sliding
[Mp]=mp_matrix(mo,L1,L1,1);%(modes,actual location of mass,
%length beam,boundary)
[Mb]=3*mb_matrix(mo,1); %(modes,boundary condition)
[BA]=(ba_matrix(mo,x1,x2,L1,1))';
%(modes,length to pzt, length to end pzt, length beam, boundary)
[Kb]=3*kb_matrix(mo,1); %(modes,boundary condition)
[BPP]=bp_matrix(mo,L1,L1,1);%(modes,actual location of mass,
%length beam,boundary)
BP=BPP';

%%%%%%%%%%%%%%%%%%%%%%%%%%%%%%
%      CONSTANTS  %
%%%%%%%%%%%%%%%%%%%%%%%%%%%%%%


Area=b*hb;    %area of aluminum cross section
palum=2.7e3; %kg/m3 for aluminum density
mb=palum*Area*L;
mp=.021; %mass of piston in kilograms
mu=mp/(3*mb); %dimensionless parameter

modes = sprintf('modes: %2.0f       poles/zeros: %2.0f',mo,po)
mass = sprintf('mass of beam: %6.4f kgs mass of piston: %6.4f kgs',mb,mp)


E=7.31e10; %N/m2  modulus for aluminum
I=(1/12)*b*hb^3; %moment of inertia for aluminum beam
d31=-320e-13; %piezoelectric strain coefficient for pzt
xo=d31*La/ha; %stress-free extension per unit volt
Y11=6.2e10; %elastic modulus
ka=wa*ha*Y11/La; %actuator stiffness
Ap=pi*((radius)*0.0254)^2; %area of piston
pair=1.16; %kg/m3 for air-density
c=343; %speed of sound in air m/s2
l=5.95*12*0.0254; %length of tube

%%%%%%%%%%%%%%%%%%%%%%%%%%%%%%%%%%%%%%%%%%%%%%%%%%%%%%%%%%%%%%%%%%%%%%%%%%%%%%%
%BUILDING OF STRUCTURAL MODE STATE SPACE MODEL
%%%%%%%%%%%%%%%%%%%%%%%%%%%%%%%%%%%%%%%%%%%%%%%%%%%%%%%%%%%%%%%%%%%%%%%%%%%%%%%

a=Ap*BP'*(pair*c^2)/(Ap*l); %grouping some terms
```

```
M=(Mb+mu*Mp); %grouping mass terms

%GROUPED TERMS IN A MATRIX
A21=-((M^-1*(E*I/(mb*L^3))*Kb)+(M^-1*(1/(mb*L))*(BA)*(ka*(hb+ha)^2)*(BA)'));

%GROUPED TERMS IN B MATRIX
%B21=[zeros(mo,1)];
B21= M^-1*(1/(mb*L))*(BA)*(xo*ka*(hb+ha));%assumes 1 volt in
B22= (-(M^-1*Ap*(1/mb)*BP));
B231= ((M^-1*Ap*(1/mb)));  %positive input pressure from external source


%NONDIMENSIONAL PARAMETERS
kappaa=(6*E*L *(1+hb/ha)^2)/(Y11*La*(hb/ha)^3);
kappat=(pair*c^2*Ap*L^3)/(E*I*l);
mu;

dimen = sprintf('Ka:  %6.3f   Kt: %6.3f   mu: %6.3f',kappaa,kappat,mu)


%DEFINING STATE SPACE MODEL
if mo >1
A=[zeros(mo,mo),eye(mo);A21,zeros(mo,mo)];
else
A=[0,1;A21,-35]; %%-35 is added damping to match data
end

B = [zeros(mo,1) zeros(mo,1);B21 B22];
C = [BP' zeros(1,mo)];
D = [0 0];


B21 = B(:,1);
B22 = B(:,2);
B23 = [0;B231];

BP3 = [1;0;0;0];




syss1=ss(A,B,C,D);

w = logspace(1,3,1000)*2*pi;

[mag1,pha1,w1]=bode(A,B,C,D,1,w);
figure
```

```
loglog(w1/2/pi,mag1/1e-6)


%%%%%%%%%%%%%%%%%%%%%%%%%%%%%%%%%%%%%%%%%%%%%%%%%%%%%%%%
% P R E S S U R E    T E R M S
%%%%%%%%%%%%%%%%%%%%%%%%%%%%%%%%%%%%%%%%%%%%%%%%%%%%%%%%


for i = 1:po
wp(i) = i*pi*c/l;
wz(i) = (2*i-1)*pi*c/(2*l);
end

num = [1 0 wz(1)^2];
den = [1 0 wp(1)^2];

for i = 1:po-1
num = conv(num,[1 0 wz(i+1)^2]);
end

anot = (pair*c^2)/(l);
numm = anot*num;

for i = 1:po-1
den = conv(den,[1 0 wp(i+1)^2]);
end

w = logspace(1,3,1000)*2*pi;

[magg,phass,w]=bode(numm,den,w);

[AaA,BbB,CcC,DdD]=tf2ss(numm,den);
press=ss(AaA,BbB,CcC,DdD);

%%positive feedback is due to the impedence term being negative
%%at lower frequencies

system= feedback(syss1,press,2,1,1);
[Aa,Bb,Cc,Dd]=ssdata(system);

S=[DdD*C CcC];  %outputs total pressure from over all system


%%IDENTIFY NEW SYSTEM WITH NEW INPUT TO IT.
Bext = [Bb [0;B231;1;zeros(2*po-1,1)]];
Dext = [0 0 0];
Bext3 = Bext(:,3);
```

```
Bext1 = Bext(:,1);




%%%%%%%%%%%%%%%%%%%%%%%%%%%%%%%%%%%%%%%%%%%%%%%%%%%%%%%%%%%%%%%%%%%%%%%%%%%%
%F U L L   S T A T E     F E E D B A C K
%%%%%%%%%%%%%%%%%%%%%%%%%%%%%%%%%%%%%%%%%%%%%%%%%%%%%%%%%%%%%%%%%%%%%%%%%%%%


eig_val=eig(Aa); %declares the poles of the fedback system
clear i %clears i from a previous usage

for q=1:length(eig(Aa)) %for loop to compute desired poles
desired_poles(q) =  (real(eig_val(q))+real(eig_val(q))-
gain)+(imag(eig_val(q))+imag(eig_val(q))*.0001)*i;
end

[eig_val desired_poles'] %prints out poles and desired poles
AC=Aa;BCB=Bext(:,1);CC=S;DCD=Dext(:,1); %renames matrices for
%full state feedback
system = ss(AC,BCB,CC,DCD); %makes into a system called "system"
g = place(Aa,BCB,desired_poles);  %calculate the desired closed loop


[magfs,phafs,w]=bode(AC-BCB*g,BCB,CC,DCD);%F S FB with voltage input
system2=ss(AC-BCB*g,BCB,CC,DCD);%creates new system with F S FB


%%%%%%%%%%%%%%%%%%%%%%%%%%%%%%%%%%%%%%%%%%%%%%%%%%%%%%%%%%%%%%%%%%%%%%%%%%%%
%F U L L     O R D E R      O B S E R V E R
%%%%%%%%%%%%%%%%%%%%%%%%%%%%%%%%%%%%%%%%%%%%%%%%%%%%%%%%%%%%%%%%%%%%%%%%%%%%


uu=length(AC); %gives size of overall matrix
yy=length(BP); %gives size of BP
olpoles = eig(Aa);


for q=1:length(eig(Aa)) %for loop to create the desired observer poles
dobpoles(q) =  (real(eig_val(q))+real(eig_val(q))gain2)+

(imag(eig_val(q))+imag(eig_val(q)*.0001))*i;
end

[olpoles dobpoles']
```

```
CCC=CC;

% When solving Ahat = A-KC => A' = A' - C'K' , then
% the transpose of K (K') is obtained.

Kt = place(Aa',CCC',dobpoles); %Obtaining the observer's gains K
K = Kt';

% Defining the Augmented System

%(coupling the observer and the system):
Aaug = [ Aa  zeros(uu,uu) ; K*CCC  Aa-K*CCC ];
Baug = [ BCB ;BCB ];
Caug = [ CCC zeros(mo,uu) ];
Daug = [ zeros(mo,1)] ;

augsys = ss(Aaug,Baug,Caug,Daug);%defines augmented system that outputs the


% Obtaining and plotting the transfer functions for the observer (output/input)
% with respect to one input only:
% the observer has 2 inputs (u and y) and "mo" outputs (displacement estimates)
% thus, to obtain tranfer functions w.r.t to input y, the other input is set
% u=0, and the state space model becomes:  qdot_hat = Ahat*xhat + K*y
%        y_hat = Chat*xhat + D*K


Aobs = Aa-K*CCC;
Bobs = K;
Cobs = CCC;
Dobs = 0;

obsys = ss(Aobs,Bobs,Cobs,Dobs);
opensys1=series(obsys,system);



%OBSERVER CLOSED LOOP

Acl = [Aa -BCB*g;K*CCC Aa-K*CCC-BCB*g];
Bcl = [Bext3;0;0;0;0;0;0];
Ccl = [[S] 0 0 0 0 0 0;0 0 0 0 0 0 [g]];
Dcl = [0;0];


clsys = ss(Acl,Bcl,Ccl,Dcl);
```

```
figure
[magext,phaext,w]=bode(Aa,Bext,S,Dext);
semilogx(w/2/pi,20*log10(abs(magext(:,3))));
grid
title('Plot of system with open loop external source vs closed loop')
ylabel('SPLout/SPLin'),xlabel('frequency, Hz');
hold on
[magcl,phacl,w]=bode(Acl,Bcl,Ccl,Dcl);
semilogx(w/2/pi,20*log10(abs(magcl(:,1))),'R');
legend('open','closed')

figure
[magext,phaext,w]=bode(Aa,Bext,S,Dext);
semilogx(w/2/pi,phaext(:,3));
grid
title('Plot of system with open loop external source vs closed loop')
ylabel('SPLout/SPLin'),xlabel('frequency, Hz');
hold on
[magcl,phacl,w]=bode(Acl,Bcl,Ccl,Dcl);
semilogx(w/2/pi,phacl(:,1),'R');
legend('open','closed')


sim('observer')

[a,b,c,d]=linmod('observer');
figure
[mag,phas,w]=bode(a,b,c,d);
semilogx(w/2/pi,mag(:,1),'R')
grid
title('external input and voltage out of observer')


[mag,phas,w]=bode(a,b,c,d);
figure
semilogx(w/2/pi,mag(:,3),'R')
grid
title('tf between input to compensator and compensator out')

figure
semilogx(w/2/pi,phas(:,3),'R')
grid
title('phase of input and output to compensator')


[mag,phas,w]=bode(a,b,c,d);
```

```
figure
semilogx(w/2/pi,20*log10(mag(:,4)),'R')
grid
title('tf between input to compensator and pressure out')


figure
semilogx(w/2/pi,phas(:,4),'R')
grid
title('tf between input to compensator and pressure out')
```

Appendix D

SIMULINK diagram for Observer

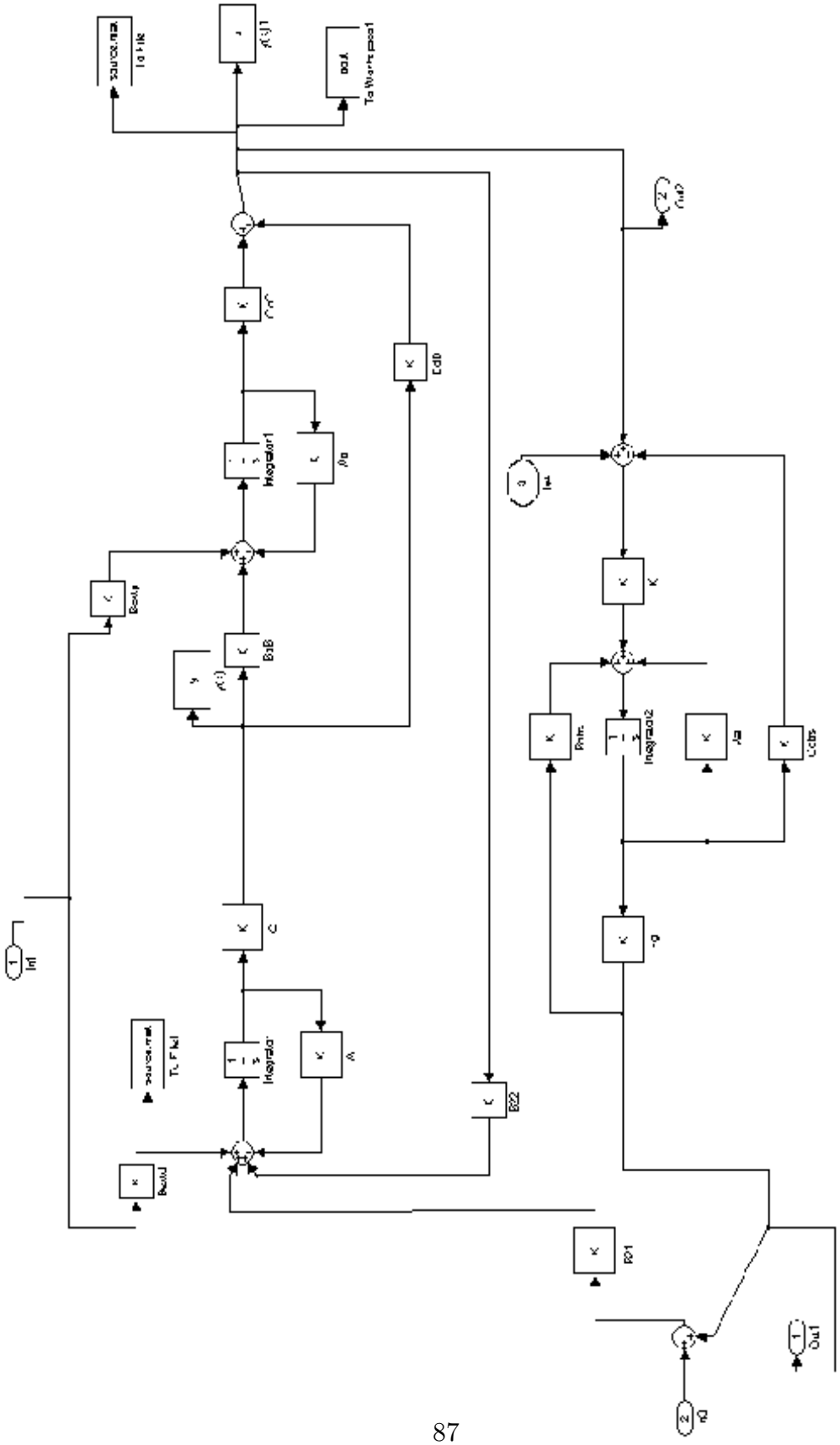

Appendix E

SIMULINK diagram for Pressure Feedback

DS1102ADC
ADC #1
ADC #2
ADC #3
ADC #4
10
Gain1
simout1
To Workspace1
Terminator
Terminator2
Terminator1
y(n)=Cx(n)+Du(n)
x(n+1)=Ax(n)+Bu(n)
Discrete State-Space1
251.5
Gain2
Scope1
y(n)=Cx(n)+Du(n)
x(n+1)=Ax(n)+Bu(n)
Discrete State-Space
Scope2
.01
Gain
simout
To Workspace
Scope
Ground
Ground1
Ground2
simout3
To Workspace2
DS1102DAC
DAC #1
DAC #2
DAC #3
DAC #4

Appendix F

SIMULINK diagram for Displacement Feedback

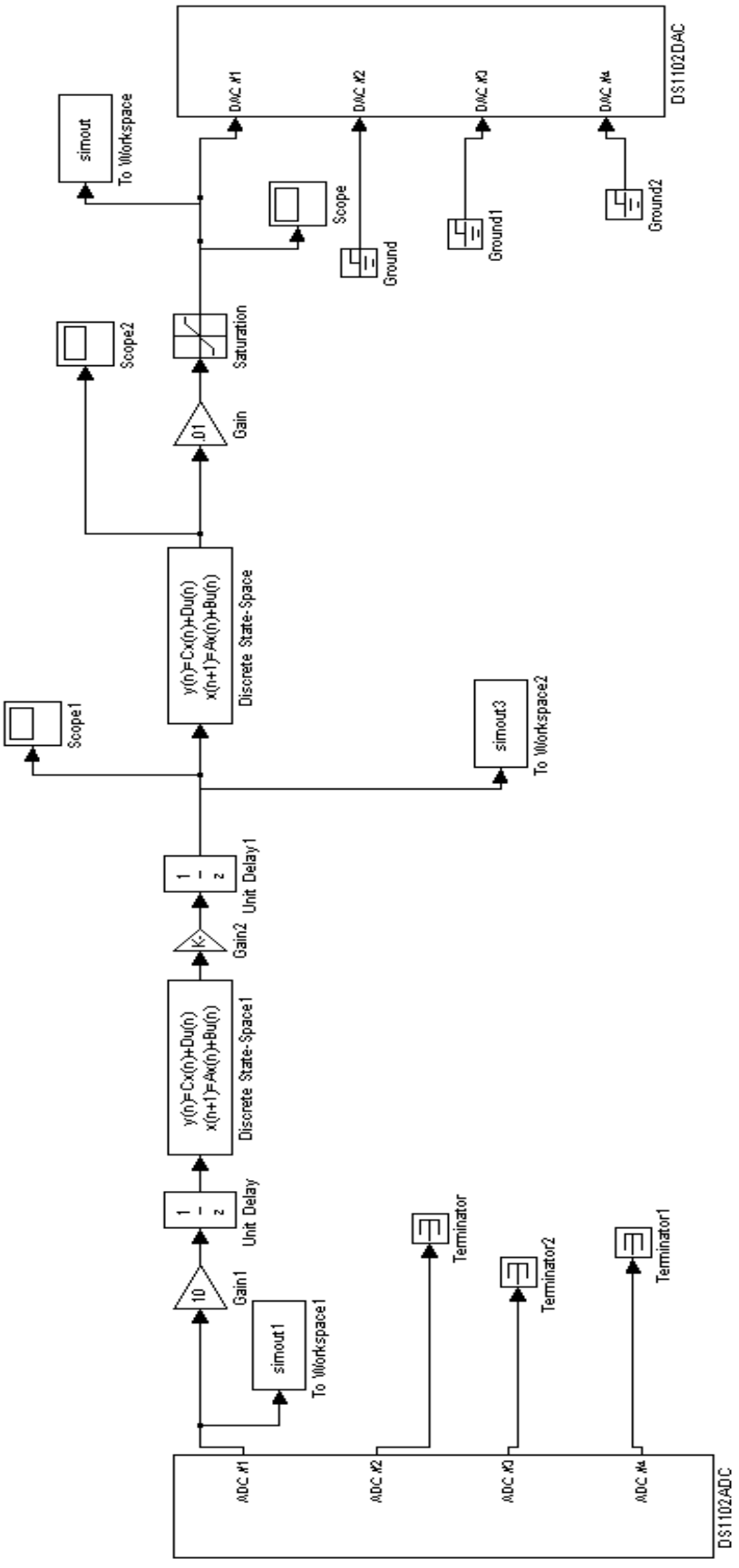
DS1102DAC
DAC #1
DAC #2
DAC #3
DAC #4
simout
To Workspace
Scope
Ground
Ground1
Ground2
Scope2
Saturation
Gain
.01
y(n)=Cx(n)+Du(n)
x(n+1)=Ax(n)+Bu(n)
Discrete State-Space
Scope1
simout3
To Workspace2
1
z
Unit Delay1
K
Gain2
Discrete State-Space1
Unit Delay
10
Gain1
simout1
To Workspace1
Terminator
Terminator2
Terminator1
ADC #1
ADC #2
ADC #3
ADC #4
DS1102ADC

Vita

The author, Kimball W. Green, son of Herman W. and Wanda M. Green, was born on September 1, 1976, in Martinsville, Virginia. He obtained his high school diploma from Bassett High School, in Bassett, Virginia, in 1994 where he was class Salutatorian. He then went to Virginia Polytechnic Institute and State University, in Blacksburg, Virginia, where he earned a Bachelor of Science in Mechanical Engineering in 1999. Staying at Virginia Tech another year, he pursued a Master of Science degree concentrating on acoustics and controls. He will work for General Motors in Baltimore, MD.

Permanent Address: 1435 John Baker Rd
Fieldale, Virginia 24089

This thesis was typeset with LaTeX 2$_\varepsilon$[1] by the author.

[1] LaTeX 2$_\varepsilon$ is an extension of LaTeX. LaTeX is a collection of macros for TeX. TeX is a trademark of the American Mathematical Society. The macros used in formatting this thesis were written by Greg Walker, Department of Mechanical Engineering, Virginia Tech.